iScience

CellPress
OPEN ACCESS

Article

Understanding cancer drug resistance with *Sleeping Beauty* functional genomic screens: Application to MAPK inhibition in cutaneous melanoma

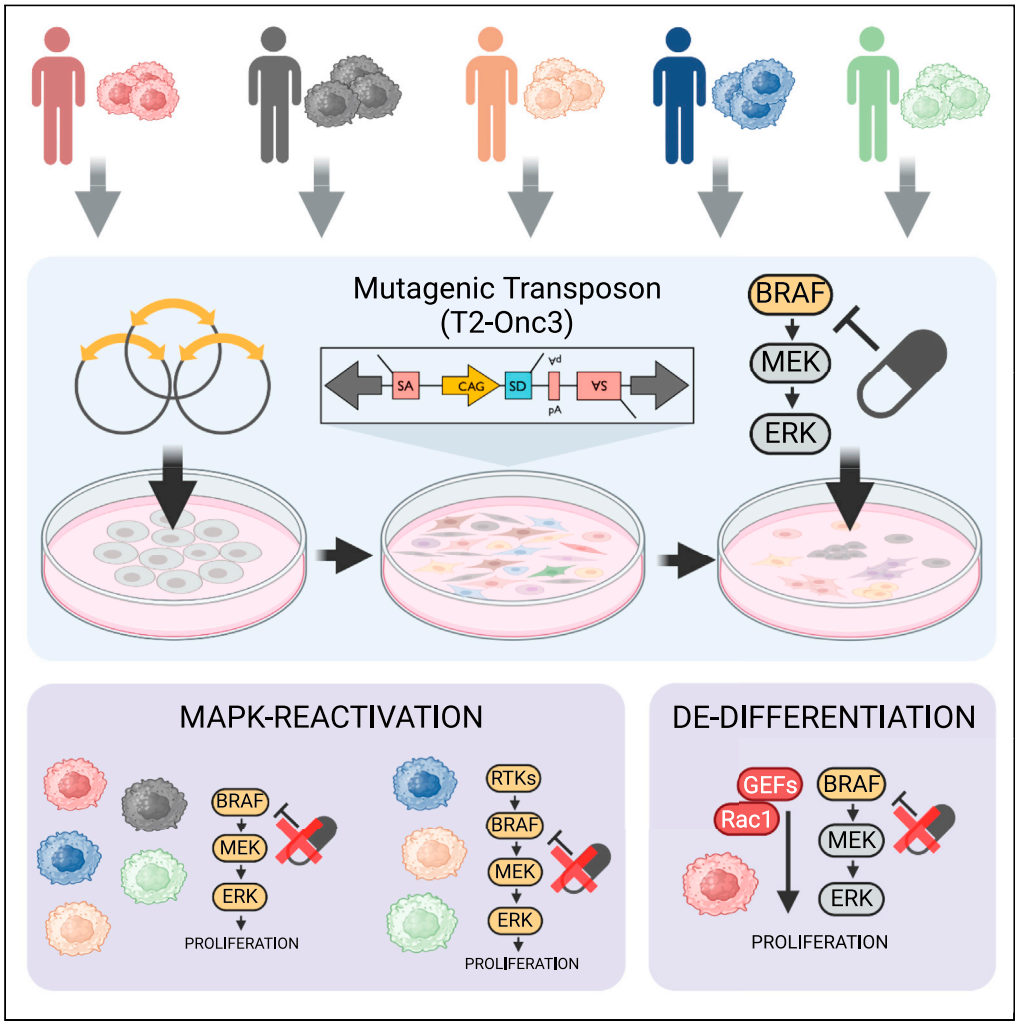

Eliot Y. Zhu, Jacob L. Schillo, Sarina D. Murray, Jesse D. Riordan, Adam J. Dupuy

adam-dupuy@uiowa.edu

Highlights

Sleeping Beauty genetic screens reveal mechanisms of cancer drug resistance

Drug resistance mechanisms are differentially utilized across melanomas

SRCi blunts BRAFi-induced transcriptional reprogramming in cutaneous melanoma

Zhu et al., iScience *26*, 107805
October 20, 2023
https://doi.org/10.1016/j.isci.2023.107805

iScience

CellPress
OPEN ACCESS

Article

Understanding cancer drug resistance with *Sleeping Beauty* functional genomic screens: Application to MAPK inhibition in cutaneous melanoma

Eliot Y. Zhu,[1,2] Jacob L. Schillo,[1,2] Sarina D. Murray,[1,2] Jesse D. Riordan,[1,2] and Adam J. Dupuy[1,2,3,*]

SUMMARY

Combined BRAF and MEK inhibition is an effective treatment for BRAF-mutant cutaneous melanoma. However, most patients progress on this treatment due to drug resistance. Here, we applied the *Sleeping Beauty* transposon system to understand how melanoma evades MAPK inhibition. We found that the specific drug resistance mechanisms differed across melanomas in our genetic screens of five cutaneous melanoma cell lines. While drivers that reactivated MAPK were highly conserved, many others were cell-line specific. One such driver, VAV1, activated a de-differentiated transcriptional program like that of hyperactive RAC1, *RAC1*^{P29S}. To target this mechanism, we showed that an inhibitor of SRC, saracatinib, blunts the VAV1-induced transcriptional reprogramming. Overall, we highlighted the importance of accounting for melanoma heterogeneity in treating cutaneous melanoma with MAPK inhibitors. Moreover, we demonstrated the utility of the *Sleeping Beauty* transposon system in understanding cancer drug resistance.

INTRODUCTION

The paradigm of directly inhibiting oncoproteins has transformed the treatment of some cancers. Small molecule inhibitors such as imatinib, which inhibits the BRC-ABL fusion protein in chronic myelogenous leukemia, or vemurafenib, which inhibits *BRAF*$^{V600E/K}$ in cutaneous melanoma, have demonstrated remarkable therapeutic efficacy with minimal adverse effects.[1,2] A recent study demonstrated that BRAF inhibitor therapy can achieve a prolonged complete response in some patients even after cessation of treatment.[3] However, the emergence of drug-resistant disease results in recurrence in most patients, even if the initial response is remarkable.[4–6] Consequently, the identification of BRAF inhibitor resistance mechanisms in melanoma has been a significant research focus.[7]

Forward genetic screens have been a workhorse for identifying drivers of drug resistance for many targeted cancer therapies.[8] Such screens involve inducing random mutations in individual cancer cells, challenging the mutagenized cells with a targeted drug to select for cells that harbor an advantageous mutation, and using high-throughput sequencing to identify the gene mutations that are enriched in drug-resistant cells.

Popular genetic screening methods utilize genetic engineering tools such as shRNA and CRISPR to manipulate gene expression. These screens require the construction of a complex library of pooled shRNA or sgRNAs that are packaged into lentivirus. To achieve genome coverage, these libraries typically contain hundreds of thousands of genetic elements.[9,10] Screens utilizing shRNA or CRISPRi induce knockdown or deletion of each gene, so the performance of individual genes is determined by the depletion of a few shRNAs or CRISPR guides that target each gene relative to the hundreds of thousands that target the other genes. Moreover, experimental conditions must be carefully controlled to ensure that most cells take up a single sgRNA/shRNA from the library to eliminate the potential for complex interactions between multiple genetic alterations. Thus, sufficient coverage of guides across all targets requires a tremendous number of cells to assess statistical significance adequately. In practice, genome-wide shRNA or CRISPR screens are difficult to perform due to the complexity of manufacturing the libraries and viral packaging, the need to mutagenize many cells to achieve uniform coverage of shRNAs or CRISPR guides, and the complexity of statistical analysis needed to account for variations in the performance of different shRNAs or CRISPR guides.

Recently, we and others have adapted the *Sleeping Beauty* (SB) transposon system to perform genetic screens in cultured cells.[11–13] Several prior studies have determined that the SB transposase exhibits little bias in selecting genomic TA sites for insertion.[14–18] This makes SB suitable for genome-wide, forward genetic screens. This approach only requires two genetic elements, the SB transposase and a mutagenic transposon (e.g., T2-Onc3), to achieve genome coverage.[12] Delivery of the transposon into cells engineered to express the SB transposase results in transposon insertion into TA dinucleotides in the host's genome. The transposon carries a promoter and splice donor and acceptor sites that enable it to induce overexpression of full-length gene transcripts or truncated forms of downstream genes.[19] Mutagenic SB

[1]Department of Anatomy and Cell Biology, Carver College of Medicine, The University of Iowa, Iowa City, IA 52242, USA
[2]Holden Comprehensive Cancer Center, The University of Iowa, Iowa City, IA 52242, USA
[3]Lead contact
*Correspondence: adam-dupuy@uiowa.edu
https://doi.org/10.1016/j.isci.2023.107805

transposons can produce gain-of-function events that are detected with less sequencing depth as compared to that of loss-of-function events introduced by shRNA or CRISPRi. This means that fewer cells need to be mutagenized to identify genes that drive a phenotype.

Around 50% of melanomas harbor the oncoprotein *BRAF*$^{V600\ E/K}$.[20] BRAF is a Raf kinase and, like other members of this protein family, participates in the MAP kinase (MAPK) signaling cascade.[21] Vemurafenib (VEM) is one of the earliest examples of a targeted inhibitor of *BRAF*$^{V600\ E/K}$ that showed remarkable therapeutic efficacy in cutaneous melanoma.[2] Since being introduced, diverse drug resistance mechanisms have been described.[22,23] We sought to model this diversity to understand how different melanomas evade BRAF inhibition (BRAFi). We performed cell-based SB mutagenesis in five *BRAF*$^{V600\ E/K}$ melanoma cell lines against encorafenib (ENCOR) and binitmetinib, which are inhibitors of BRAF and MEK, respectively.[24–31] Compared to VEM, ENCOR binds more strongly to *BRAF*$^{V600\ E/K}$, which translated to improved overall survival compared to VEM in a clinical trial.[32]

SB mutagenesis identified drivers of drug resistance in five melanoma cell lines. We observed that both the specific candidates and the overall number of candidates differed across cell lines. BRAF was the most conserved candidate. Other candidates involved in MAPK signaling included HGF, KRAS, and the receptor tyrosine kinases (RTKs) PDGFRB and CSF1R. Potentially independent from MAPK, VAV1, a GEF for Rho family GTPases, drove a de-differentiated transcriptional program like that of hyperactive Rac1, *RAC1*^{P29S}. This upregulation of a de-differentiated gene set could be blunted by the inhibitor of SRC, saracatinib (SARA). Collectively, our data suggest divergence in the utilization of different drug resistance mechanisms across melanomas, which highlights the need for a precision approach to overcome drug resistance to MAPK inhibition. Furthermore, our study demonstrates the utility of the SB system in understanding cancer drug resistance.

RESULTS

Sleeping Beauty genetic screens inform diversity of resistance mechanisms to MAPK inhibition in cutaneous melanoma

We screened five *BRAF*$^{V600\ E/K}$ melanoma cell lines (A375, COLO858, UACC62, UACC257, and PDX10) for drivers of drug resistance to combined BRAF/MEK inhibition (Figure 1A). The melanoma cell lines were engineered to express the SB100X transposase (Figure S1).[33] Mutagenesis was achieved by transfection of pT2-Onc3.[30,34,35] Each screen was initiated in approximately thirty million SB mutagenized cancer cells seeded across 10cm plates with one million cells per plate. Targeted transposon junction sequencing in cells remaining after 3–5 weeks of BRAF/MEK inhibition revealed enrichment of transposons near genes of interest. Statistical significance was determined using a chi-squared test based on the number of integrations in a gene and the number of observed TAs in each gene-associated region.[18] We also compared insertion profiles in selected samples to that of cells that did not undergo drug selection. More details on the insertion site analysis can be obtained from our previous paper.[31]

After 3–5 weeks of drug selection, macroscopic colonies were observed in plates with mutagenized cells to varying degrees (Figure S2). We observed non-uniform genome coverage of transposons in unselected samples that were altered by drug selection (Figure 1B). The non-uniformity of coverage in unselected samples could be attributed to mapping artifacts or regions of the genome in the cancer cell lines with copy number gains. Our analysis pipeline uses the reference genome to assess statistical significance. Thus, biologically significant events may not be statistically significant, or vice versa. The *BRAF* locus resides on chromosome 7, and drug selection enriches for insertions in *BRAF* for most cell lines (Figure 1B). The genomic coverage of the screen differed across cell lines, with UACC257 harboring the greatest number of transposons per plate following transfection and five days of treatment with DMSO, the drug vehicle (VEH) (Figure 1C).

To assess screen saturation, we took random subsets of plates and determined the number of true positive drivers that could be detected using each subset. True positive drivers are defined as those that survived the filtering step after analysis of the entire dataset. In theory, the number of drivers should increase with the number of plates. However, we found that the number of drivers did not noticeably change for COLO858 and PDX10 between using the smallest subset of five drug-selected plates versus the entire dataset. Moreover, COLO858 and PDX10 had fewer drivers than A375 and UACC257 (Figure 1D). While the transfection and DNA amplification protocols used to screen each cell line could impact the number of detected drivers, the data from A375 and COLO858 show a comparable degree of mutagenesis according to their insertion profiles (Figures 1C–1E). Despite this, these two cell lines had notably different performances. Increasing the size of the COLO858 dataset had a minimal impact on the number of drivers identified. By contrast, increasing the number of mutagenized A375 samples correlated with an increase in the number of drivers identified (Figure 1D). This observation was particularly notable given that the COLO858 screen showed greater coverage (i.e., # of genes mutated) relative to A375 (Figure 1C).

In terms of specific genes, truncated BRAF emerged as a significant candidate in all but one cell line (Figure 1E). Truncated BRAF works by reactivating MAPK by forming drug-resistant dimers.[36] Deletion of exons 2–8 is the analogous mutation seen in patients.[37] We have previously demonstrated that overexpression of truncated BRAF or CRAF strongly drives resistance to BRAFi in a panel of *BRAF*$^{V600\ E/K}$ melanoma cell lines.[11] We found other potential activators of MAPK such as PDGFRB and CSF1R in some cell lines. PDGFRB and CSF1R are both RTKs that partly drive drug resistance due to MAPK-reactivation.[38–40] Other MAPK-associated candidates were truncated CRAF (*RAF1*) and HGF (Figure 1E).

A pharmacologic strategy to inhibit RAF-dimer-dependent drug resistance is pan-Raf inhibitors.[41,42] To identify drivers of pan-RAF inhibitors, we screened A375 and COLO858 with the pan-RAF inhibitor LY3009120. Compared to our BRAF/MEK screen, pan-RAF inhibition favored the overexpression of full-length BRAF over truncated BRAF. Furthermore, truncated ARAF emerged as a candidate in the pan-RAF inhibitor screen for both A375 and COLO858 (Figure S3A). We attempted to validate truncated ARAF. However, cells with verified overexpression of truncated ARAF were not more drug-resistant to pan-RAF inhibition (Figures S3B and S3C).

VAV1, a DBL-family guanine exchange factor (GEF), emerged only in A375 (Figure 1E). In A375, we also hit the GEFs VAV2 and MCF2. We previously identified VAV1 as a driver of drug resistance to VEM in A375 as a proof-of-concept for our *in vitro* SB mutagenesis method.[11,12] The

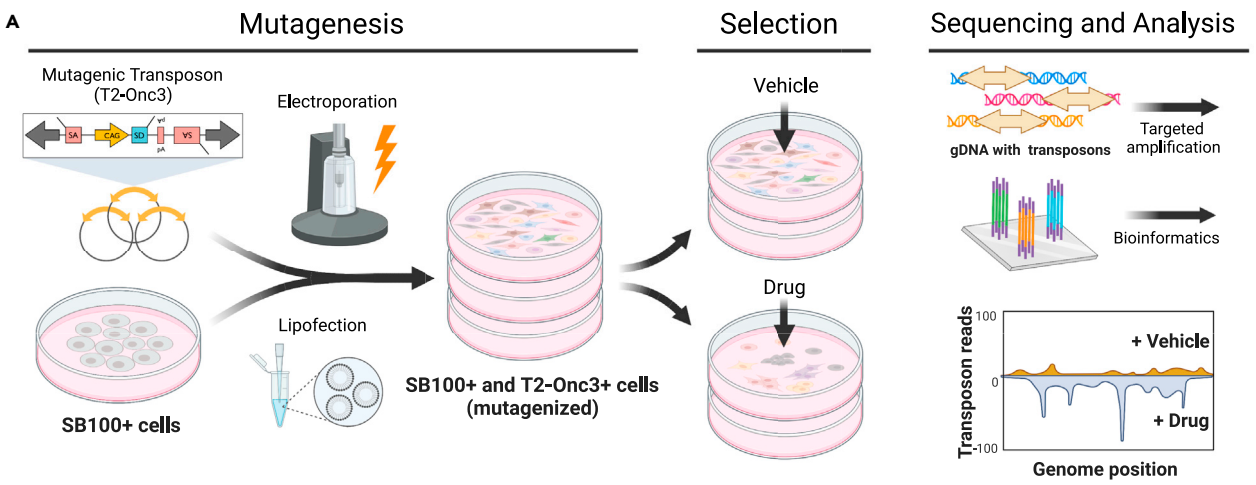
A
Mutagenesis
Selection
Sequencing and Analysis
Mutagenic Transposon
(T2-Onc3)
Electroporation
Lipofection
SB100+ cells
SB100+ and T2-Onc3+ cells
(mutagenized)
Vehicle
Drug
gDNA with transposons
Targeted
amplification
Bioinformatics
Transposon reads
+ Vehicle
+ Drug
Genome position

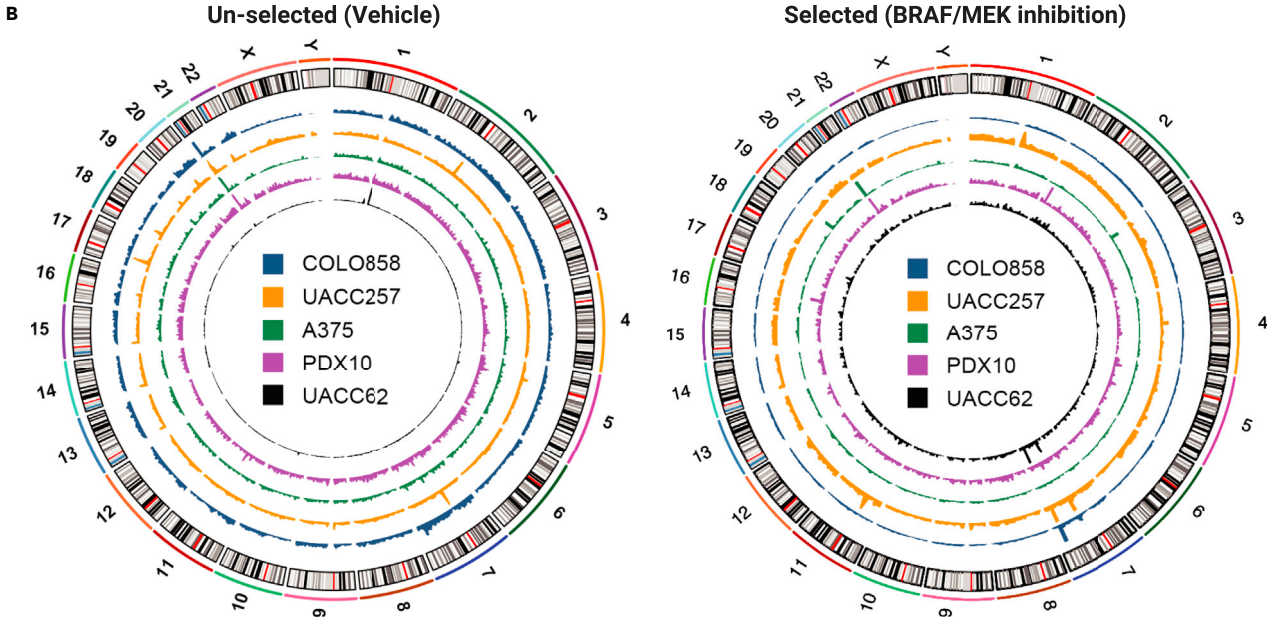
B
Un-selected (Vehicle)
Selected (BRAF/MEK inhibition)
COLO858
UACC257
A375
PDX10
UACC62

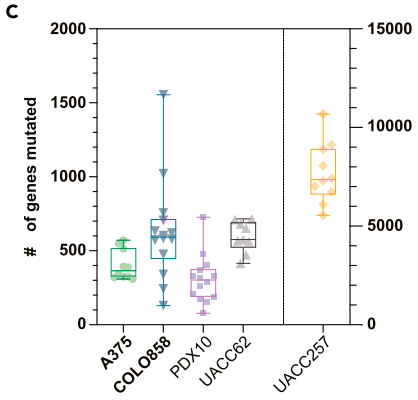
C
# of genes mutated
A375
COLO858
PDX10
UACC62
UACC257

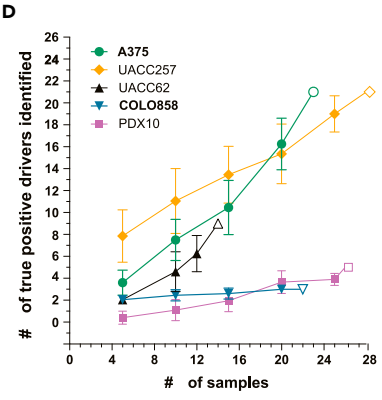
D
# of true positive drivers identified
# of samples
A375
UACC257
UACC62
COLO858
PDX10

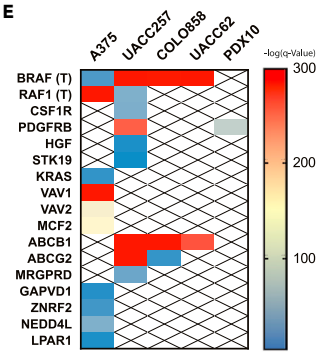
E
A375
UACC257
COLO858
UACC62
PDX10
-log(q-Value)
BRAF (T)
RAF1 (T)
CSF1R
PDGFRB
HGF
STK19
KRAS
VAV1
VAV2
MCF2
ABCB1
ABCG2
MRGPRD
GAPVD1
ZNRF2
NEDD4L
LPAR1

Figure 1. *Sleeping Beauty* genetic screen strategy and melanoma BRAF/MEK inhibition screen results

(A) Schematic of the genetic screens.

(B) Circos plot of insertion sites in unselected samples (left) and BRAF/MEKi selected samples (right). Each ring displays data from the screen for a given cell line.

(C) Boxplots showing the number of unique genes mutated per 10cm plate for a given cell line screen. The right Y axis is for UACC257 data. The edges of the boxes denote the 1st and 3rd quartiles, and the line denotes the 2nd quartile.

(D) Line plot showing the number of true positive drivers detected when using a subset of n samples. The X axis denotes n. True positive drivers are those that passed filtering when using the entire dataset. The error bars denote the 95% confidence interval.

(E) Heatmap of the -log(q-value) for select candidates recovered in our genetic screens. The q value is the multi-hypothesis corrected p value generated by performing a chi-squared test based on the observed number of insertions in a gene and the expected number of insertions in a gene. The expected number of insertions is derived from the number of TA sites in a gene and the total number of insertions in the dataset.

precise way in which these GEFs drive drug resistance is not known. We speculated that it depends on the activation of Rac1.[11] The only other recurrent drivers we observed were the presumed drug efflux pumps ABCB1 and ABCG2, which have been shown to drive drug resistance to BRAFi in cutaneous melanoma.[43–45] A complete list of candidates is provided in Table S1. Genomic map of insertions for BRAF, VAV1, PDGFRB, and CSF1R observed in our screen are shown in Figure 2. Overall, these results suggest that melanomas have different potentials to evade BRAFi and favor different resistance mechanisms.

Candidates perform non-uniformly across melanomas

Next, we sought to validate a subset of candidates that we identified. We wondered if the our screen results would predict a candidate's ability to drive drug resistance in certain cell lines. We focused our attention on VAV1, CSF1R, and PDGFRB. Based on prior studies, we proposed a mechanism for each candidate in Figure 3A. We previously showed that overexpression of *VAV1* leads to increased GTP-bound RAC1.[11] RTKs drive MAPK signaling, and past studies have shown that PDGFRB and CSF1R promote resistance to BRAFi in melanoma by restoring phospho-ERK. We tested the ability of these candidates to drive drug resistance to ENCOR and the MEK inhibitor, cobimetinib (COBI), in the melanoma cell lines A375, 451Lu, SKMEL28, and PDX10. We found that VAV1 drove drug resistance to BRAFi and MEKi in all the cell lines we tested (Figures 3C and 3D). However, VAV1 also suppressed the growth in standard conditions for some cell lines, including SKMEL28 and PDX10 (Figure 3E). When normalized to cells on day zero rather than VEH-treated cells on day three or four, overexpression of *VAV1* did not increase viability in ENCOR compared to EM-expressing cells for SKMEL28 and PDX10 (Figure 3E). This result suggests that some cell lines may not utilize the RAC1 resistance mechanism because it suppresses the growth of parental cell lines. A375 and 451Lu can be distinguished from the other cell lines based on the expression of the de-differentiated transcriptional program.[46]

PDGFRB and CSF1R also inconsistently increased resistance to BRAFi and MEKi in the panel of melanomas we tested (Figures 3C and 3D). The inability of the RTKs to drive drug resistance may be due to a lack of ligand expression by a given cell line to drive autocrine signaling. Thus, we tested ligand-independent versions of PDGFRB (*PDGFRB*^{N666K}) and CSF1R (*CSF1R*$^{L301S,\ Y969}$) in A375, where overexpression of WT copies of these RTKs only modestly increased drug resistance.[47,48] Indeed, *PDGFRB*^{N666K} and *CSF1R*$^{L301S,\ Y969}$ greatly outperformed their WT counterparts in increasing viability and sustaining phospho-ERK signaling in ENCOR (Figures 3F and 3G). This result indicates that divergence in cell-secreted ligands adds to the complexity of which drug resistance mechanisms are relevant for a given melanoma.

De-differentiation engages different mechanisms of drug resistance and can be targeted with SRC inhibition

We previously showed that overexpression of *VAV1* increases RAC1 signaling and promotes drug resistance to BRAFi in cutaneous melanoma.[11,46,49,50] To determine the overlap between VAV1 and RAC1 signaling, we performed RNA-seq on A375 with enforced expression of *VAV1* or *RAC1*^{P29S} (Figure 4A). The *RAC1*^{P29S} mutation is observed in ~3% of cutaneous melanomas and encodes a hyperactive form of RAC1 that drives BRAFi resistance and metastasis in cutaneous melanoma.[20,51–54] We observed that VAV1 and *RAC1*^{P29S} drove the Tsoi Un-differentiated gene expression signature (Figure 4A). There was also a high degree of overlap between enriched MSigDB Hallmark pathways and differentially expressed genes (Figures 4B and 4C). Finally, we confirmed that enforced expression of *VAV1* increased protein levels of CAV1 and AXL, two proteins associated with melanoma de-differentiation (Figure S4A). In general, the de-differentiated subtype of melanoma is more resistant to BRAFi.[46,55–62] This result suggests that VAV1 engages a RAC1-mediated transcriptional program, leading to a BRAFi-resistant phenotypic state.

We also previously showed that A375 with enforced expression of *VAV1* could be sensitized to BRAFi with SARA, a selective inhibitor of SRC.[11] To understand SARA's mechanisms of action, we performed RNA-seq on *VAV1*-overexpressing A375 treated with SARA. We saw that SARA blunted genes upregulated by VAV1, including those that define the de-differentiated transcriptional state (Figures 4D and 4E). To identify other drugs that could suppress the de-differentiated transcriptional program, we computed the similarity between LINCs L1000 chemical perturbation consensus signatures and genes upregulated by *VAV1* and *RAC1*^{P29S} and those that define the de-differentiated melanoma subtype. The LINCs L1000 chemical perturbation signatures are pre-computed gene expression profiles of 1000 genes generated from cancer cell lines treated with different compounds.[63] We used the Enrichr webtool to rank over 10,000 signatures for each of the gene sets.[64–66] We found these sets of genes most overlapped with those suppressed by dasatinib, another inhibitor of SRC (Figure 4F). The entire list of genes differentially expressed upon *RAC1*^{P29S} and *VAV1* overexpression compared to empty vector and SRCi compared to *VAV1* overexpression is provided in Table S2.

The de-differentiated cutaneous melanoma subtype is widely appreciated to be more drug-resistant to BRAFi. However, this subtype is characterized by elevated expression of hundreds of genes, many of which may not promote drug resistance. We wondered if our screen

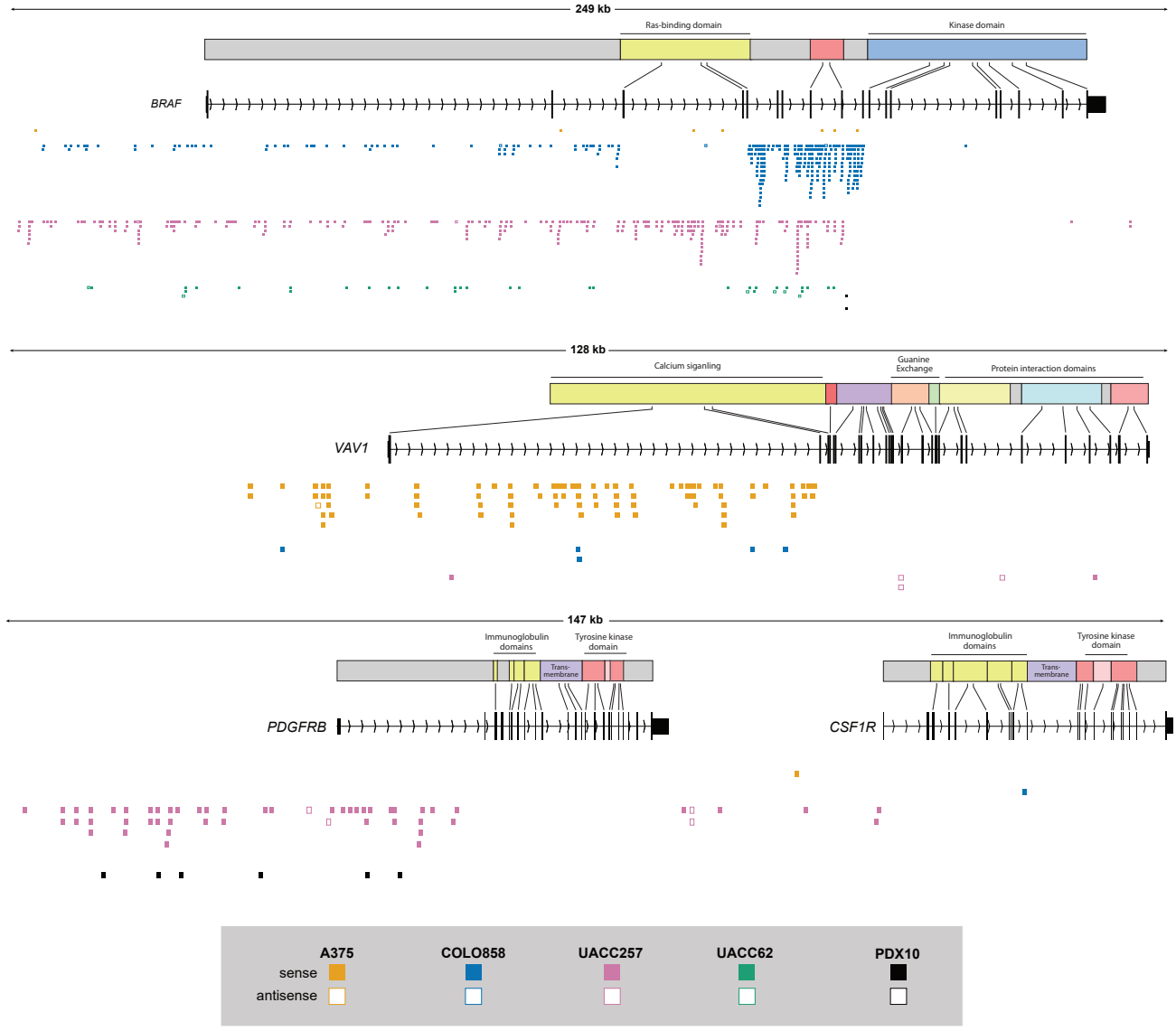

Figure 2. Genomic map of insertions in select candidates

Each rectangle denotes a detected transposon in a sample. Rectangles are colored based on the cell line it belonged to. Rectangles are solid if the direction of the CAG promoter in the transposon is sense to the gene orientation. Otherwise, the CAG promoter in the transposon is anti-sense to the gene orientation.

candidates were among those upregulated in de-differentiated melanomas. We mined the TCGA cutaneous melanoma dataset and found that the expression of *CSF1R*, *PDGFRB*, and *ABCB1* was elevated in de-differentiated melanomas (Figure 4G). This observation is consistent with the finding that PDGFRB and CSF1R are under the control of TEADs, a known driver of de-differentiation in cutaneous melanoma.[67] Interestingly, we saw that the ligands for CSF1R and PDGFRB, apart from IL34, were also elevated in de-differentiated melanomas (Figure S4B). Finally, the enforced expression of *VAV1* or *RAC1*^{P29S} led to a modest but statistically significant (adjusted p value <0.01) increase in the expression of *ABCB1* and *ABCG2* (Figure 4H). Together, these findings suggest that de-differentiated melanomas are more resistant to BRAFi partly due to their ability to maintain MAPK through RTKs and drug efflux pumps.

DISCUSSION

Targeted BRAF/MEK inhibition is a safe and effective treatment option for patients with metastatic *BRAF*$^{V600\ E/K}$ cutaneous melanoma. However, only around 20% of patients achieve durable responses.[68] Diverse resistance mechanisms have been reported, but no framework exists to target these mechanisms. In this study, we used *in vitro* SB genetic screens to model the diverse ways melanomas evade BRAFi.

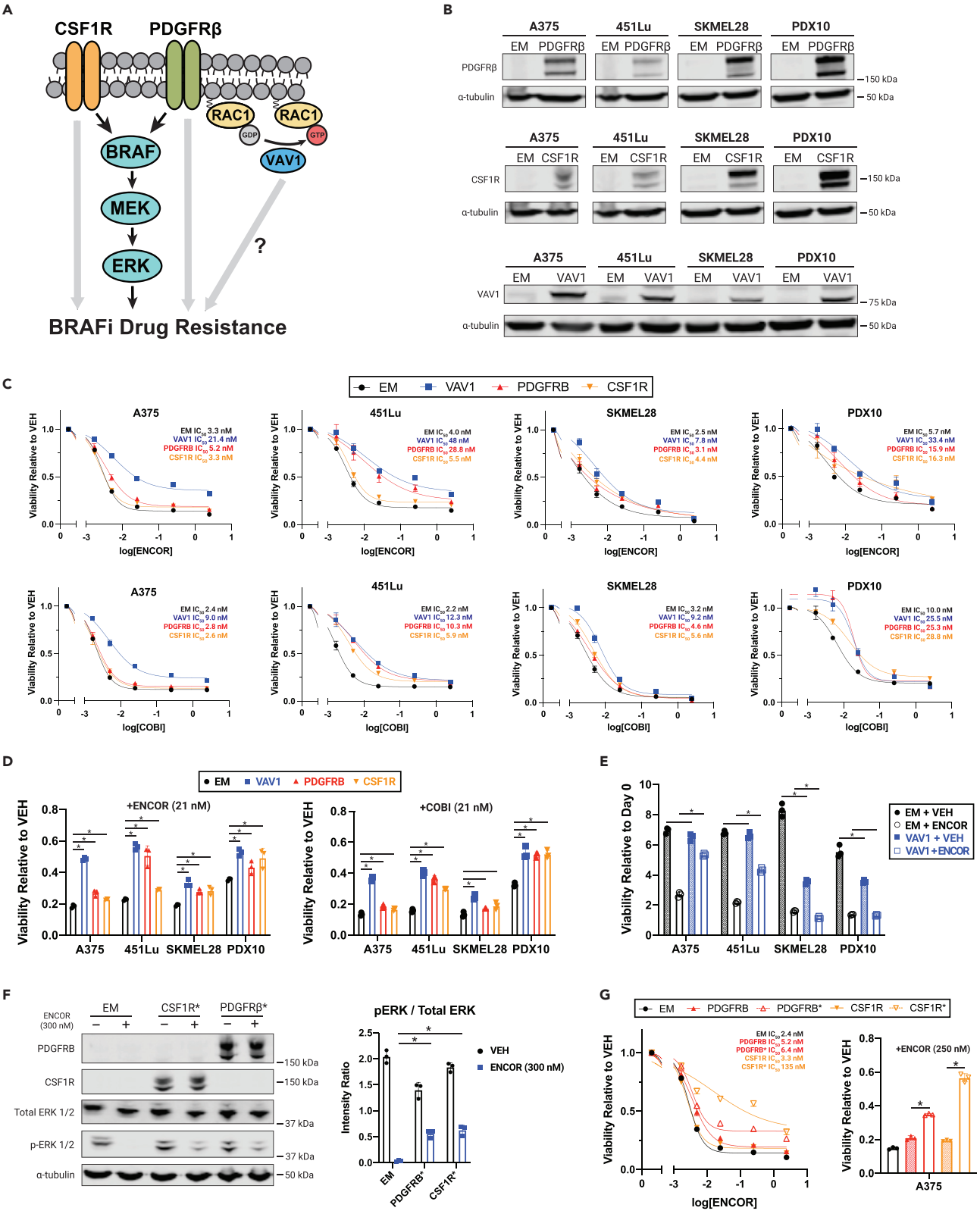
A
CSF1R
PDGFRβ
RAC1
RAC1
GDP
GTP
VAV1
BRAF
MEK
ERK
?
BRAFi Drug Resistance
B
A375
451Lu
SKMEL28
PDX10
EM PDGFRβ
PDGFRβ
α-tubulin
150 kDa
50 kDa
EM CSF1R
CSF1R
EM VAV1
VAV1
75 kDa
C
EM
VAV1
PDGFRB
CSF1R
Viability Relative to VEH
log[ENCOR]
log[COBI]
D
+ENCOR (21 nM)
+COBI (21 nM)
E
Viability Relative to Day 0
EM + VEH
EM + ENCOR
VAV1 + VEH
VAV1 + ENCOR
F
ENCOR (300 nM)
PDGFRB
CSF1R
Total ERK 1/2
p-ERK 1/2
α-tubulin
pERK / Total ERK
Intensity Ratio
VEH
ENCOR (300 nM)
G
PDGFRB*
CSF1R*
+ENCOR (250 nM)

Figure 3. Performance of candidates

(A) Schematic of potential mechanisms by which candidates drive drug resistance.

(B) Representative western blot with indicated antibodies in a panel of melanoma cell lines engineered to overexpress the screen candidates, empty vector (EM), VAV1, PDGFRB, or CSF1R.

(C) Dose-response of modified cell lines against ENCOR and COBI. Top row shows ENCOR data and bottom row shows COBI data. Each data point represents three replicate measurements. Viability is shown after three days of drug treatment for A375 and 451Lu and four days for SKMEL28 and PDX10. The error bars denote the 95% confidence interval.

(D) Alternate visualization of data in (C) showing viability of indicated cell lines relative to VEH for 21 nM of ENCOR or COBI. Asterix indicates two-tailed Welch's t-test p value of <0.05. The error bars denote the 95% confidence interval.

(E) Viability of indicated cell lines relative to day zero after three days for A375 and 451Lu and four days for SKMEL28 and PDX10. Conditions included either treatment with VEH or ENCOR. Asterix indicates two-tailed Welch's t-test p value of <0.05. The error bars denote the 95% confidence interval.

(F) Representative western blot for indicated antibodies in A375 modified with enforced expression of empty vector (EM), *CSF1R* $^{L301S,\ Y969}$ (CSF1R*), and *PDGFRB*^{N666K} (PDGFRB*). Cells were treated either VEH or 300nm of ENCOR for 6 h. Right panel shows quantification of three technical replicate blots. Asterix indicates two-tailed Welch's t-test p value of <0.05. The error bars denote the 95% confidence interval.

(G) Dose-response curves of A375 modified with EM, CSF1R*, and PDGFRB* against ENCOR. Right panel is alternate visualization that displays data from dose-response curves for 21 nM of ENCOR. Asterix indicates two-tailed Welch's t-test p value of <0.05. The error bars denote the 95% confidence interval.

MAPK-reactivation is seen in approximately half of patients who progressed on BRAFi.[56,69] Consistent with this observation, SB revealed that truncated BRAF and CRAF were the most conserved drivers across the melanomas we screened (Figure 1E). Other genomic BRAF alterations including focal amplifications can also drive MAPK-reactivation.[70,71] Another way to restore MAPK signaling during BRAFi is through activating RTKs. RTKs can activate MAPK by promoting Ras activation to drive formations of RAF hetero/homo dimers that do not efficiently bind selective BRAF inhibitors. In the same vein, activating mutations in NRAS, which lies downstream of RTKs, drive drug resistance to BRAFi in cutaneous melanoma.[40]

Our screen highlighted two RTKs, PDGFRB and CSF1R, which have been shown to drive drug resistance to BRAFi in cutaneous melanoma.[38–40] However, overexpression of these RTKs did not uniformly promote drug resistance, suggesting that targeting RTKs may not overcome drug resistance in some melanomas. Mechanistically, the inability of the RTKs to drive drug resistance may be due to a lack of ligand expression by a given cell line. In support of this hypothesis, the constitutively active versions of these RTKs significantly increased the viability of A375 in ENCOR compared to overexpression of the WT versions of these RTKs (Figure 3G). This finding is consistent with previous studies that showed that RTKs such as AXL, and NGFR, while elevated in drug-resistant cells, do not remarkably alter response.[58,72] Finally, our screens also revealed HGF, a ligand for c-MET. Upregulation of c-MET is a clinically observed and validated driver of resistance to BRAFi in melanoma.[56]

Beyond MAPK-reactivation, some melanomas withstand BRAFi by undergoing phenotype switching.[40,58,61,72–77] In general, de-differentiated melanomas are less dependent on ERK signaling.[54,56,57] The de-differentiated transcriptional program includes the overexpression of thousands of genes, and it is not clear which genes promote drug resistance.[40,58,61,72–76] Our analysis suggests that upregulation of RTKs, their ligands, and drug efflux pumps may help de-differentiated melanomas maintain the minimal level of MAPK signaling needed to survive BRAFi.

RAC1^{P29S} drives de-differentiation in cutaneous melanomas and promotes resistance to BRAFi and ERKi.[46,53,54,78] In melanomas with RAC1 activating mutations, VAV1 can elicit a de-differentiation gene expression profile like that of *RAC1*^{P29S} (Figures 4A–4C). However, the ability of VAV1 to promote drug resistance is not universal. Our SB screens revealed that VAV1 is the preferred driver of drug resistance in A375 but not in the other cell lines we screened (Figure 1E). For cell lines such as PDX10 and SKMEL28, *VAV1* overexpression suppressed growth in standard conditions and did not provide a growth advantage during BRAFi (Figure 3E). We have previously demonstrated that a key difference between these cell lines is that A375 and 451Lu belong to the de-differentiated molecular subtype of cutaneous melanoma, characterized by the high protein abundance of AXL and CAV1.[46]

To target de-differentiation, we have previously shown that SRCi suppresses the expression of de-differentiation genes in melanomas and increases the efficacy of BRAFi.[46] SRC is a critical transducer of cellular signaling from growth factor receptors and integrins.[79] Here, we showed that SRCi could blunt the enforced upregulation of the de-differentiated transcriptomic program elicited by *VAV1* overexpression. This result is consistent with the finding that SRCi blunts the upregulation of de-differentiation genes during BRAFi in some melanomas.[58] Dasatinib, a non-specific inhibitor of SRC, may also suppress de-differentiation based on our LINCs L1000 consensus drug signature analysis (Figure 4F). We and others have shown that dasatinib enhances the efficacy of BRAFi in several melanoma cell lines.[46,74] In integrin signaling, SRC cooperates with FAK to regulate actin cytoskeleton dynamics and cellular adhesion.[80] FAKi have also been shown to be effective for targeting BRAFi-resistant melanomas that are de-differentiated.[62,81]

Pan-Raf inhibitors can block the activity of BRAF-dimers. When we screened melanomas against pan-RAF inhibition, truncated ARAF and full-length BRAF was more statistically significance than truncated BRAF. However, overexpression of the kinase domain of ARAF failed to drive drug resistance to the pan-Raf inhibitor, LY3009120, (Figure S3). We speculate that cooperating mutations are necessary for the function of truncated ARAF. In our screen, a single mutagenized cell can contain upwards of 20 transposons.[12] Nevertheless, a previous study has shown that mutations in the ARAF kinase domain drive resistance to the pan-RAF inhibitor, Belvarafenib, in a dimer and kinase-dependent fashion, in melanoma.[82]

While resistance mechanisms can be described based on their ability to restore MAPK, it is important to remember that melanomas can undergo both non-genomic and genomic evolution during drug selection.[56,76] BRAFi selects a rare population of slow-cycling cells that undergo de-differentiation.[58,76] These slow-cycling cells sustain increased DNA damage, which enables the acquisition of genomic alterations

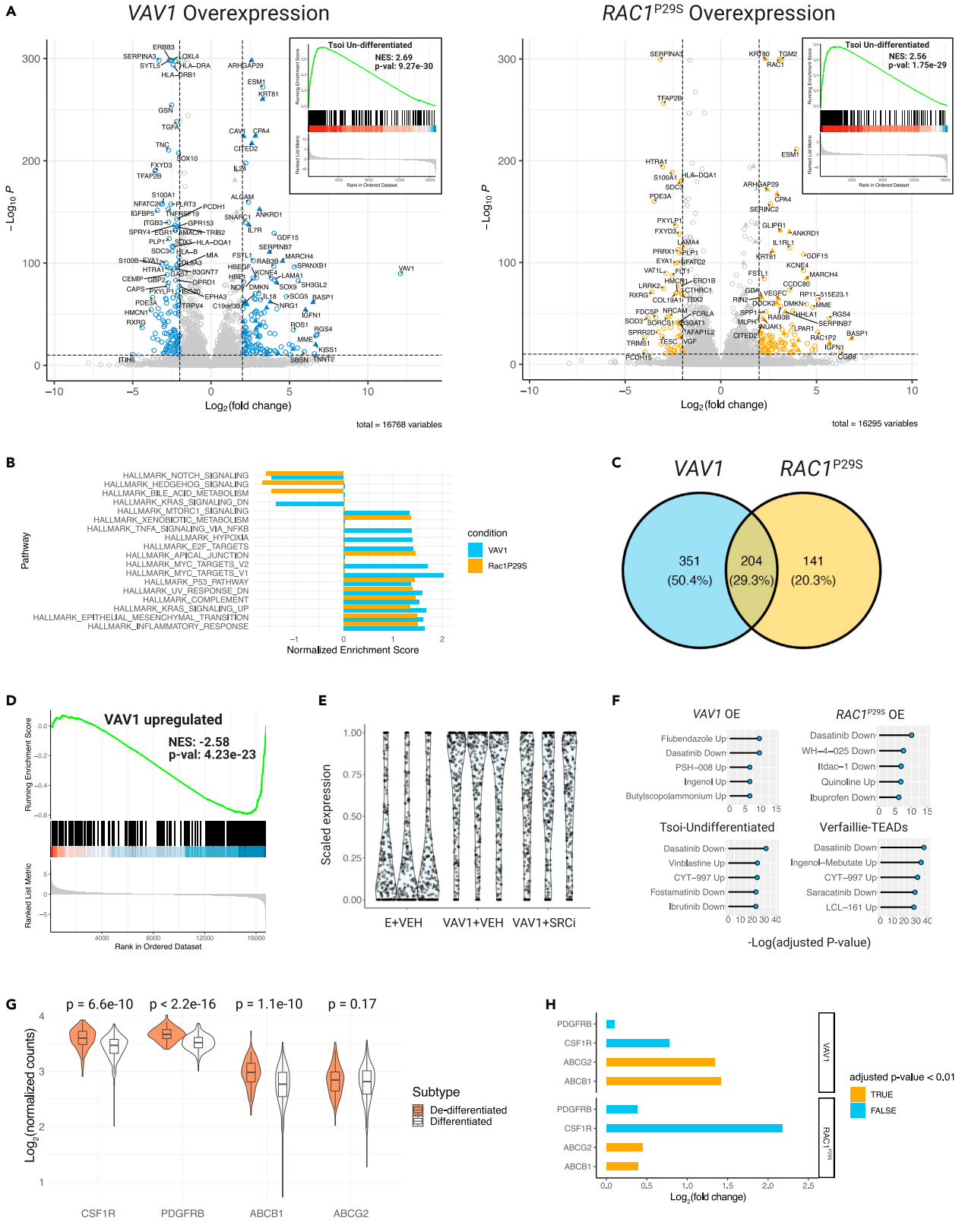
A
VAV1 Overexpression
RAC1P29S Overexpression
Tsoi Un-differentiated
NES: 2.69
p-val: 9.27e-30
Tsoi Un-differentiated
NES: 2.56
p-val: 1.75e-29
−Log10 P
Log2(fold change)
total = 16768 variables
total = 16295 variables
B
Pathway
HALLMARK_NOTCH_SIGNALING
HALLMARK_HEDGEHOG_SIGNALING
HALLMARK_BILE_ACID_METABOLISM
HALLMARK_KRAS_SIGNALING_DN
HALLMARK_MTORC1_SIGNALING
HALLMARK_XENOBIOTIC_METABOLISM
HALLMARK_TNFA_SIGNALING_VIA_NFKB
HALLMARK_HYPOXIA
HALLMARK_E2F_TARGETS
HALLMARK_APICAL_JUNCTION
HALLMARK_MYC_TARGETS_V2
HALLMARK_MYC_TARGETS_V1
HALLMARK_P53_PATHWAY
HALLMARK_UV_RESPONSE_DN
HALLMARK_COMPLEMENT
HALLMARK_KRAS_SIGNALING_UP
HALLMARK_EPITHELIAL_MESENCHYMAL_TRANSITION
HALLMARK_INFLAMMATORY_RESPONSE
Normalized Enrichment Score
condition
VAV1
Rac1P29S
C
VAV1
RAC1P29S
351
(50.4%)
204
(29.3%)
141
(20.3%)
D
VAV1 upregulated
NES: -2.58
p-val: 4.23e-23
Running Enrichment Score
Ranked List Metric
Rank in Ordered Dataset
E
Scaled expression
E+VEH
VAV1+VEH
VAV1+SRCi
F
VAV1 OE
RAC1P29S OE
Flubendazole Up
Dasatinib Down
PSH−008 Up
Ingenol Up
Butylscopolammonium Up
Dasatinib Down
WH−4−025 Down
Itdac−1 Down
Quinoline Up
Ibuprofen Down
Tsoi-Undifferentiated
Dasatinib Down
Vinblastine Up
CYT−997 Up
Fostamatinib Down
Ibrutinib Down
Verfaillie-TEADs
Dasatinib Down
Ingenol−Mebutate Up
CYT−997 Up
Saracatinib Down
LCL−161 Up
-Log(adjusted P-value)
G
p = 6.6e-10
p < 2.2e-16
p = 1.1e-10
p = 0.17
Log2(normalized counts)
CSF1R
PDGFRB
ABCB1
ABCG2
Subtype
De-differentiated
Differentiated
H
PDGFRB
CSF1R
ABCG2
ABCB1
VAV1
RAC1
adjusted p-value < 0.01
TRUE
FALSE
Log2(fold change)

Figure 4. VAV1 drives phenotype switching by engaging a RAC1-like transcriptional program

(A) Volcano plot of differentially expressed genes induced by enforced expression of *VAV1* (left) or *RAC1*^{P29S} (right) in A375. Solid triangles are genes that belong to the Tsoi Un-differentiated gene set. Top right of each volcano plot shows GSEA enrichment of the Tsoi-Undifferentiated gene set in the entire list of genes.
(B) GSEA normalized enrichment scores of MSigDB Hallmark pathways in genes differentially expressed by enforced expression of *VAV1* or *RAC1*^{P29S} in A375.
(C) Venn diagram showing the overlap of genes differentially expressed by the enforced expression of *VAV1* or *RAC1*^{P29S} in A375. Only genes with an adjusted p value of <0.01 and abs(log_2FC) > 2 are included.
(D) Enrichment of gene set upregulated by enforced expression of *VAV1* in genes differentially expressed upon saracatinib treatment.
(E) Violin plots of scaled expression values of genes in Tsoi-Undifferentiated gene set in A375 with empty vector and treated with vehicle (E + VEH), A375 with enforced *VAV1* expression and treated with vehicle (VAV1+VEH), and A375 with enforced expression of *VAV1* treated with saracatinib (VAV1+SRCi).
(F) Top five similar LINCs L1000 chemical perturbation consensus signatures identified by Enrichr for genes overexpressed with *VAV1* and *RAC1*^{P29S} and genes in the Tsoi-Undifferentiated and Verfaillie-TEADs gene sets. Overexpression is defined as adjusted p value of <0.01 and log_2FC > 2. OE stands for overexpression.
(G) Violin plot of normalized expression of indicated genes in de-differentiated and differentiated melanomas in the TCGA SKCM dataset (n = 472, de-differentiated = 85). P-value was computed using Welch's t-test. Significance was determined using a p value cutoff of 0.05. The edges of the boxes denote the 1st and 3rd quartiles, and the line denotes the 2nd quartile.
(H) log_2FC and adjusted p value of indicated genes elicited by overexpression of *VAV1* or *RAC1*^{P29S}.

that can restore MAPK.[83] In one study, slow-cycling de-differentiated melanoma overcame FAK inhibition, which selectively targets this population, with mutations that reactivated ERK.[62]

In summary, our study demonstrates the utility of SB insertional mutagenesis of cultured cells to understand cancer drug resistance. For BRAFi in cutaneous melanoma, our screens revealed the two main classes of drug resistance involving either MAPK-reactivation or lineage plasticity. The breadth of our screens has shown that melanomas have different potentials to become drug-resistant and disparate utilization of specific resistance mechanisms across cell lines (Figures 1D, 1E, and 3E). Collectively, our work underscores the importance of taking a precision approach to overcoming drug resistance to MAPK inhibition in cutaneous melanoma. Practically, specific drug combinations need to be created for different resistance mechanisms. Such drug combinations should address mechanisms that arise from the reactivation of MAPK and the activation of parallel pathways. Since these mechanisms are not universal, developing biomarkers that predict which resistance mechanisms a melanoma will utilize would greatly enhance therapy response.

Limitations of the study

- Our genetic screens are performed in cultured cells. Numerous factors, including the stiffness of the extracellular matrix, are different *in vivo*. Thus, there may be more resistance mechanisms that are engaged *in vivo* that we may not have identified.
- We used bulk sequencing to characterize the transposons in our samples. Thus, we are unable to determine cooperation and/or interactions between different transposon-induced mutations.
- Our validation experiments are performed during a short time frame of less than a week. Candidates may not perform the same during more extended periods of drug treatment.
- The SB system is biased toward identifying gain-of-function events as mutagenesis of only one allele of a gene results in the phenotype. By contrast, disruption of all alleles of a gene is required for loss-of-function events. The advantage of identifying gain-of-function mutations is that they are more actionable since most cancer drugs are designed to inhibit targets of interest.

STAR★METHODS

Detailed methods are provided in the online version of this paper and include the following:

- KEY RESOURCES TABLE
- RESOURCE AVAILABILITY
  - Lead contact
  - Materials availability
  - Data and code availability
- EXPERIMENTAL MODEL AND STUDY PARTICIPANT DETAILS
  - Cell lines
- METHOD DETAILS
  - *Sleeping beauty* genetic screens
  - Library preparation and sequencing
  - Cell staining
  - RT-qPCR
  - Enforced expression of candidates
  - Viability assays
  - Inhibitors
  - Immunoblotting
- QUANTIFICATION AND STATISTICAL ANALYSIS

- RNAseq analysis
- Transposon insertion site analysis
- TCGA analysis
- Statistical analysis

SUPPLEMENTAL INFORMATION

Supplemental information can be found online at https://doi.org/10.1016/j.isci.2023.107805.

ACKNOWLEDGMENTS

This study was funded by NIH NCI (F30 CA247102), the UIOWA Medical Scientist Training Program, (NIH NIGMS T32 GM007337), The Melanoma Research Foundation Medical Student Award, The American Skin Association Medical Student Award (E.Y.Z.), The Iowa Department of Public Health Melanoma Research Award (A.D.), The Mezhir Award, and Core facilities at the University of Iowa supported by grant P30 CA086862 to the Holden Comprehensive Cancer Center (A.D.).

AUTHOR CONTRIBUTIONS

E.Y.Z. and A.J.D. conceived the project. E.Y.Z. wrote the manuscript and performed most of the experiments. E.Y.Z and A.J.D. performed the sequencing analysis. J.D.R. and J.L.S. performed library preparation for A375 and COLO858 screens. S.D.M. performed the western blot confirming VAV1-induced changes in protein abundance. All authors contributed to manuscript revisions.

DECLARATION OF INTERESTS

The authors declare no competing interests.

Received: February 27, 2023
Revised: July 10, 2023
Accepted: August 29, 2023
Published: August 31, 2023

REFERENCES

1. Iqbal, N., and Iqbal, N. (2014). Imatinib: a breakthrough of targeted therapy in cancer. Chemother. Res. Pract. *2014*, 357027. https://doi.org/10.1155/2014/357027.
2. Chapman, P.B., Hauschild, A., Robert, C., Haanen, J.B., Ascierto, P., Larkin, J., Dummer, R., Garbe, C., Testori, A., Maio, M., et al. (2011). Improved survival with vemurafenib in melanoma with BRAF V600E mutation. N. Engl. J. Med. *364*, 2507–2516. https://doi.org/10.1056/NEJMoa1103782.
3. Warburton, L., Meniawy, T.M., Calapre, L., Pereira, M., McEvoy, A., Ziman, M., Gray, E.S., and Millward, M. (2020). Stopping targeted therapy for complete responders in advanced BRAF mutant melanoma. Sci. Rep. *10*, 18878. https://doi.org/10.1038/s41598-020-75837-5.
4. Boumahdi, S., and de Sauvage, F.J. (2020). The great escape: tumour cell plasticity in resistance to targeted therapy. Nat. Rev. Drug Discov. *19*, 39–56. https://doi.org/10.1038/s41573-019-0044-1.
5. Groenendijk, F.H., and Bernards, R. (2014). Drug resistance to targeted therapies: deja vu all over again. Mol. Oncol. *8*, 1067–1083. https://doi.org/10.1016/j.molonc.2014.05.004.
6. Sabnis, A.J., and Bivona, T.G. (2019). Principles of Resistance to Targeted Cancer Therapy: Lessons from Basic and Translational Cancer Biology. Trends Mol. Med. *25*, 185–197. https://doi.org/10.1016/j.molmed.2018.12.009.
7. Villanueva, J., Vultur, A., and Herlyn, M. (2011). Resistance to BRAF inhibitors: unraveling mechanisms and future treatment options. Cancer Res. *71*, 7137–7140. https://doi.org/10.1158/0008-5472.CAN-11-1243.
8. Noorani, I., Bradley, A., and de la Rosa, J. (2020). CRISPR and transposon *in vivo* screens for cancer drivers and therapeutic targets. Genome Biol. *21*, 204. https://doi.org/10.1186/s13059-020-02118-9.
9. Sims, D., Mendes-Pereira, A.M., Frankum, J., Burgess, D., Cerone, M.A., Lombardelli, C., Mitsopoulos, C., Hakas, J., Murugaesu, N., Isacke, C.M., et al. (2011). High-throughput RNA interference screening using pooled shRNA libraries and next generation sequencing. Genome Biol. *12*, R104. https://doi.org/10.1186/gb-2011-12-10-r104.
10. Shalem, O., Sanjana, N.E., Hartenian, E., Shi, X., Scott, D.A., Mikkelson, T., Heckl, D., Ebert, B.L., Root, D.E., Doench, J.G., and Zhang, F. (2014). Genome-scale CRISPR-Cas9 knockout screening in human cells. Science *343*, 84–87. https://doi.org/10.1126/science.1247005.
11. Feddersen, C.R., Schillo, J.L., Varzavand, A., Vaughn, H.R., Wadsworth, L.S., Voigt, A.P., Zhu, E.Y., Jennings, B.M., Mullen, S.A., Bobera, J., et al. (2019). Src-Dependent DBL Family Members Drive Resistance to Vemurafenib in Human Melanoma. Cancer Res. *79*, 5074–5087. https://doi.org/10.1158/0008-5472.CAN-19-0244.
12. Feddersen, C.R., Wadsworth, L.S., Zhu, E.Y., Vaughn, H.R., Voigt, A.P., Riordan, J.D., and Dupuy, A.J. (2019). A simplified transposon mutagenesis method to perform phenotypic forward genetic screens in cultured cells. BMC Genom. *20*, 497. https://doi.org/10.1186/s12864-019-5888-6.
13. O'Donnell, K.A., Guo, Y., Suresh, S., Updegraff, B.L., and Zhou, X. (2019). Ex Vivo Transposon-Mediated Genetic Screens for Cancer Gene Discovery. Methods Mol. Biol. *1907*, 145–157. https://doi.org/10.1007/978-1-4939-8967-6_12.
14. Liang, Q., Kong, J., Stalker, J., and Bradley, A. (2009). Chromosomal mobilization and reintegration of Sleeping Beauty and PiggyBac transposons. Genesis *47*, 404–408. https://doi.org/10.1002/dvg.20508.
15. Vigdal, T.J., Kaufman, C.D., Izsvák, Z., Voytas, D.F., and Ivics, Z. (2002). Common physical properties of DNA affecting target site selection of sleeping beauty and other Tc1/mariner transposable elements. J. Mol. Biol. *323*, 441–452. https://doi.org/10.1016/s0022-2836(02)00991-9.
16. Woodard, L.E., Li, X., Malani, N., Kaja, A., Hice, R.H., Atkinson, P.W., Bushman, F.D., Craig, N.L., and Wilson, M.H. (2012). Comparative analysis of the recently discovered hAT transposon TcBuster in human cells. PLoS One *7*, e42666. https://doi.org/10.1371/journal.pone.0042666.
17. Yant, S.R., Wu, X., Huang, Y., Garrison, B., Burgess, S.M., and Kay, M.A. (2005). High-resolution genome-wide mapping of transposon integration in mammals. Mol. Cell Biol. *25*, 2085–2094. https://doi.org/10.1128/MCB.25.6.2085-2094.2005.
18. Brett, B.T., Berquam-Vrieze, K.E., Nannapaneni, K., Huang, J., Scheetz, T.E., and Dupuy, A.J. (2011). Novel molecular and computational methods improve the accuracy of insertion site analysis in Sleeping Beauty-induced tumors. PLoS One *6*, e24668.

https://doi.org/10.1371/journal.pone.0024668.

19. Guimaraes-Young, A., Feddersen, C.R., and Dupuy, A.J. (2019). Sleeping Beauty Mouse Models of Cancer: Microenvironmental Influences on Cancer Genetics. Front. Oncol. *9*, 611. https://doi.org/10.3389/fonc.2019.00611.
20. Cancer Genome Atlas Research Network, Weinstein, J.N., Collisson, E.A., Mills, G.B., Shaw, K.R.M., Ozenberger, B.A., Ellrott, K., Shmulevich, I., Sander, C., and Stuart, J.M. (2013). The Cancer Genome Atlas Pan-Cancer analysis project. Nat. Genet. *45*, 1113–1120. https://doi.org/10.1038/ng.2764.
21. Wellbrock, C., Karasarides, M., and Marais, R. (2004). The RAF proteins take centre stage. Nat. Rev. Mol. Cell Biol. *5*, 875–885. https://doi.org/10.1038/nrm1498.
22. Luebker, S.A., and Koepsell, S.A. (2019). Diverse Mechanisms of BRAF Inhibitor Resistance in Melanoma Identified in Clinical and Preclinical Studies. Front. Oncol. *9*, 268. https://doi.org/10.3389/fonc.2019.00268.
23. Proietti, I., Skroza, N., Bernardini, N., Tolino, E., Balduzzi, V., Marchesiello, A., Michelini, S., Volpe, S., Mambrin, A., Mangino, G., et al. (2020). Mechanisms of Acquired BRAF Inhibitor Resistance in Melanoma: A Systematic Review. Cancers *12*, 2801. https://doi.org/10.3390/cancers12102801.
24. Ivics, Z., Hackett, P.B., Plasterk, R.H., and Izsvák, Z. (1997). Molecular reconstruction of Sleeping Beauty, a Tc1-like transposon from fish, and its transposition in human cells. Cell *91*, 501–510.
25. Heasman, S.J., and Ridley, A.J. (2008). Mammalian Rho GTPases: new insights into their functions from *in vivo* studies. Nat. Rev. Mol. Cell Biol. *9*, 690–701. https://doi.org/10.1038/nrm2476.
26. Rogers, L.M., Olivier, A.K., Meyerholz, D.K., and Dupuy, A.J. (2013). Adaptive immunity does not strongly suppress spontaneous tumors in a Sleeping Beauty model of cancer. J. Immunol. *190*, 4393–4399. https://doi.org/10.4049/jimmunol.1203227.
27. Berquam-Vrieze, K.E., Nannapaneni, K., Brett, B.T., Holmfeldt, L., Ma, J., Zagorodna, O., Jenkins, N.A., Copeland, N.G., Meyerholz, D.K., Knudson, C.M., et al. (2011). Cell of origin strongly influences genetic selection in a mouse model of T-ALL. Blood *118*, 4646–4656. https://doi.org/10.1182/blood-2011-03-343947.
28. Riordan, J.D., Feddersen, C.R., Tschida, B.R., Beckmann, P.J., Keng, V.W., Linden, M.A., Amin, K., Stipp, C.S., Largaespada, D.A., and Dupuy, A.J. (2018). Chronic liver injury alters driver mutation profiles in hepatocellular carcinoma in mice. Hepatology *67*, 924–939. https://doi.org/10.1002/hep.29565.
29. Riordan, J.D., Keng, V.W., Tschida, B.R., Scheetz, T.E., Bell, J.B., Podetz-Pedersen, K.M., Moser, C.D., Copeland, N.G., Jenkins, N.A., Roberts, L.R., et al. (2013). Identification of rtl1, a retrotransposon-derived imprinted gene, as a novel driver of hepatocarcinogenesis. PLoS Genet. *9*, e1003441. https://doi.org/10.1371/journal.pgen.1003441.
30. Dupuy, A.J., Rogers, L.M., Kim, J., Nannapaneni, K., Starr, T.K., Liu, P., Largaespada, D.A., Scheetz, T.E., Jenkins, N.A., and Copeland, N.G. (2009). A modified sleeping beauty transposon system that can be used to model a wide variety of human cancers in mice. Cancer Res. *69*, 8150–8156. https://doi.org/10.1158/0008-5472.CAN-09-1135.
31. Riordan, J.D., Drury, L.J., Smith, R.P., Brett, B.T., Rogers, L.M., Scheetz, T.E., and Dupuy, A.J. (2014). Sequencing methods and datasets to improve functional interpretation of sleeping beauty mutagenesis screens. BMC Genom. *15*, 1150. https://doi.org/10.1186/1471-2164-15-1150.
32. Dummer, R., Ascierto, P.A., Gogas, H.J., Arance, A., Mandala, M., Liszkay, G., Garbe, C., Schadendorf, D., Krajsova, I., Gutzmer, R., et al. (2018). Encorafenib plus binimetinib versus vemurafenib or encorafenib in patients with BRAF-mutant melanoma (COLUMBUS): a multicentre, open-label, randomised phase 3 trial. Lancet Oncol. *19*, 603–615. https://doi.org/10.1016/S1470-2045(18)30142-6.
33. Mátés, L., Chuah, M.K.L., Belay, E., Jerchow, B., Manoj, N., Acosta-Sanchez, A., Grzela, D.P., Schmitt, A., Becker, K., Matrai, J., et al. (2009). Molecular evolution of a novel hyperactive Sleeping Beauty transposase enables robust stable gene transfer in vertebrates. Nat. Genet. *41*, 753–761. https://doi.org/10.1038/ng.343.
34. Dupuy, A.J., Akagi, K., Largaespada, D.A., Copeland, N.G., and Jenkins, N.A. (2005). Mammalian mutagenesis using a highly mobile somatic Sleeping Beauty transposon system. Nature *436*, 221–226. https://doi.org/10.1038/nature03691.
35. Collier, L.S., Carlson, C.M., Ravimohan, S., Dupuy, A.J., and Largaespada, D.A. (2005). Cancer gene discovery in solid tumours using transposon-based somatic mutagenesis in the mouse. Nature *436*, 272–276. https://doi.org/10.1038/nature03681.
36. Poulikakos, P.I., Persaud, Y., Janakiraman, M., Kong, X., Ng, C., Moriceau, G., Shi, H., Atefi, M., Titz, B., Gabay, M.T., et al. (2011). RAF inhibitor resistance is mediated by dimerization of aberrantly spliced BRAF(V600E). Nature *480*, 387–390. https://doi.org/10.1038/nature10662.
37. Johnson, D.B., Childress, M.A., Chalmers, Z.R., Frampton, G.M., Ali, S.M., Rubinstein, S.M., Fabrizio, D., Ross, J.S., Balasubramanian, S., Miller, V.A., et al. (2018). BRAF internal deletions and resistance to BRAF/MEK inhibitor therapy. Pigment Cell Melanoma Res. *31*, 432–436. https://doi.org/10.1111/pcmr.12674.
38. Giricz, O., Mo, Y., Dahlman, K.B., Cotto-Rios, X.M., Vardabasso, C., Nguyen, H., Matusow, B., Bartenstein, M., Polishchuk, V., Johnson, D.B., et al. (2018). The RUNX1/IL-34/CSF-1R axis is an autocrinally regulated modulator of resistance to BRAF-V600E inhibition in melanoma. JCI Insight *3*, e120422. https://doi.org/10.1172/jci.insight.120422.
39. Shi, H., Kong, X., Ribas, A., and Lo, R.S. (2011). Combinatorial treatments that overcome PDGFRbeta-driven resistance of melanoma cells to V600EB-RAF inhibition. Cancer Res. *71*, 5067–5074. https://doi.org/10.1158/0008-5472.CAN-11-0140.
40. Nazarian, R., Shi, H., Wang, Q., Kong, X., Koya, R.C., Lee, H., Chen, Z., Lee, M.K., Attar, N., Sazegar, H., et al. (2010). Melanomas acquire resistance to B-RAF(V600E) inhibition by RTK or N-RAS upregulation. Nature *468*, 973–977. https://doi.org/10.1038/nature09626.
41. Peng, S.B., Henry, J.R., Kaufman, M.D., Lu, W.P., Smith, B.D., Vogeti, S., Rutkoski, T.J., Wise, S., Chun, L., Zhang, Y., et al. (2015). Inhibition of RAF Isoforms and Active Dimers by LY3009120 Leads to Anti-tumor Activities in RAS or BRAF Mutant Cancers. Cancer Cell *28*, 384–398. https://doi.org/10.1016/j.ccell.2015.08.002.
42. Cook, F.A., and Cook, S.J. (2021). Inhibition of RAF dimers: it takes two to tango. Biochem. Soc. Trans. *49*, 237–251. https://doi.org/10.1042/BST20200485.
43. Wu, C.P., Sim, H.M., Huang, Y.H., Liu, Y.C., Hsiao, S.H., Cheng, H.W., Li, Y.Q., Ambudkar, S.V., and Hsu, S.C. (2013). Overexpression of ATP-binding cassette transporter ABCG2 as a potential mechanism of acquired resistance to vemurafenib in BRAF(V600E) mutant cancer cells. Biochem. Pharmacol. *85*, 325–334. https://doi.org/10.1016/j.bcp.2012.11.003.
44. Durmus, S., Sparidans, R.W., Wagenaar, E., Beijnen, J.H., and Schinkel, A.H. (2012). Oral availability and brain penetration of the B-RAFV600E inhibitor vemurafenib can be enhanced by the P-GLYCOprotein (ABCB1) and breast cancer resistance protein (ABCG2) inhibitor elacridar. Mol. Pharm. *9*, 3236–3245. https://doi.org/10.1021/mp3003144.
45. Wu, C.P., and V Ambudkar, S. (2014). The pharmacological impact of ATP-binding cassette drug transporters on vemurafenib-based therapy. Acta Pharm. Sin. B *4*, 105–111. https://doi.org/10.1016/j.apsb.2013.12.001.
46. Zhu, E.Y., Riordan, J.D., Vanneste, M., Henry, M.D., Stipp, C.S., and Dupuy, A.J. (2022). SRC-RAC1 signaling drives drug resistance to BRAF inhibition in de-differentiated cutaneous melanomas. npj Precis. Oncol. *6*, 74. https://doi.org/10.1038/s41698-022-00310-7.
47. Sletta, K.Y., Castells, O., and Gjertsen, B.T. (2021). Colony Stimulating Factor 1 Receptor in Acute Myeloid Leukemia. Front. Oncol. *11*, 654817. https://doi.org/10.3389/fonc.2021.654817.
48. Arts, F.A., Chand, D., Pecquet, C., Velghe, A.I., Constantinescu, S., Hallberg, B., and Demoulin, J.B. (2016). PDGFRB mutants found in patients with familial infantile myofibromatosis or overgrowth syndrome are oncogenic and sensitive to imatinib. Oncogene *35*, 3239–3248. https://doi.org/10.1038/onc.2015.383.
49. Vanneste, M., Feddersen, C.R., Varzavand, A., Zhu, E.Y., Foley, T., Zhao, L., Holt, K.H., Milhem, M., Piper, R., Stipp, C.S., et al. (2020). Functional Genomic Screening Independently Identifies CUL3 as a Mediator of Vemurafenib Resistance via Src-Rac1 Signaling Axis. Front. Oncol. *10*, 442. https://doi.org/10.3389/fonc.2020.00442.
50. Zhu, E.Y., and Dupuy, A.J. (2022). Machine learning approach informs biology of cancer drug response. BMC Bioinf. *23*, 184. https://doi.org/10.1186/s12859-022-04720-z.
51. Davis, M.J., Ha, B.H., Holman, E.C., Halaban, R., Schlessinger, J., and Boggon, T.J. (2013). RAC1P29S is a spontaneously activating cancer-associated GTPase. Proc. Natl. Acad. Sci. USA *110*, 912–917. https://doi.org/10.1073/pnas.1220895110.
52. Kawazu, M., Ueno, T., Kontani, K., Ogita, Y., Ando, M., Fukumura, K., Yamato, A., Soda, M., Takeuchi, K., Miki, Y., et al. (2013). Transforming mutations of RAC guanosine triphosphatases in human cancers. Proc. Natl. Acad. Sci. USA *110*, 3029–3034. https://doi.org/10.1073/pnas.1216141110.
53. Watson, I.R., Li, L., Cabeceiras, P.K., Mahdavi, M., Gutschner, T., Genovese, G., Wang, G., Fang, Z., Tepper, J.M., Stemke-Hale, K., et al. (2014). The RAC1 P29S hotspot mutation in melanoma confers resistance to

pharmacological inhibition of RAF. Cancer Res. *74*, 4845–4852. https://doi.org/10.1158/0008-5472.CAN-14-1232-T.

54. Mohan, A.S., Dean, K.M., Isogai, T., Kasitinon, S.Y., Murali, V.S., Roudot, P., Groisman, A., Reed, D.K., Welf, E.S., Han, S.J., et al. (2019). Enhanced Dendritic Actin Network Formation in Extended Lamellipodia Drives Proliferation in Growth-Challenged Rac1(P29S) Melanoma Cells. Dev. Cell *49*, 444–460.e9. https://doi.org/10.1016/j.devcel.2019.04.007.
55. Tsoi, J., Robert, L., Paraiso, K., Galvan, C., Sheu, K.M., Lay, J., Wong, D.J.L., Atefi, M., Shirazi, R., Wang, X., et al. (2018). Multi-stage Differentiation Defines Melanoma Subtypes with Differential Vulnerability to Drug-Induced Iron-Dependent Oxidative Stress. Cancer Cell *33*, 890–904.e5. https://doi.org/10.1016/j.ccell.2018.03.017.
56. Hugo, W., Shi, H., Sun, L., Piva, M., Song, C., Kong, X., Moriceau, G., Hong, A., Dahlman, K.B., Johnson, D.B., et al. (2015). Non-genomic and Immune Evolution of Melanoma Acquiring MAPKi Resistance. Cell *162*, 1271–1285. https://doi.org/10.1016/j.cell.2015.07.061.
57. Song, C., Piva, M., Sun, L., Hong, A., Moriceau, G., Kong, X., Zhang, H., Lomeli, S., Qian, J., Yu, C.C., et al. (2017). Recurrent Tumor Cell-Intrinsic and -Extrinsic Alterations during MAPKi-Induced Melanoma Regression and Early Adaptation. Cancer Discov. *7*, 1248–1265. https://doi.org/10.1158/2159-8290.CD-17-0401.
58. Fallahi-Sichani, M., Becker, V., Izar, B., Baker, G.J., Lin, J.R., Boswell, S.A., Shah, P., Rotem, A., Garraway, L.A., and Sorger, P.K. (2017). Adaptive resistance of melanoma cells to RAF inhibition via reversible induction of a slowly dividing de-differentiated state. Mol. Syst. Biol. *13*, 905. https://doi.org/10.15252/msb.20166796.
59. Su, Y., Wei, W., Robert, L., Xue, M., Tsoi, J., Garcia-Diaz, A., Homet Moreno, B., Kim, J., Ng, R.H., Lee, J.W., et al. (2017). Single-cell analysis resolves the cell state transition and signaling dynamics associated with melanoma drug-induced resistance. Proc. Natl. Acad. Sci. USA *114*, 13679–13684. https://doi.org/10.1073/pnas.1712064115.
60. Tirosh, I., Izar, B., Prakadan, S.M., Wadsworth, M.H., 2nd, Treacy, D., Trombetta, J.J., Rotem, A., Rodman, C., Lian, C., Murphy, G., et al. (2016). Dissecting the multicellular ecosystem of metastatic melanoma by single-cell RNA-seq. Science *352*, 189–196. https://doi.org/10.1126/science.aad0501.
61. Müller, J., Krijgsman, O., Tsoi, J., Robert, L., Hugo, W., Song, C., Kong, X., Possik, P.A., Cornelissen-Steijger, P.D.M., Geukes Foppen, M.H., et al. (2014). Low MITF/AXL ratio predicts early resistance to multiple targeted drugs in melanoma. Nat. Commun. *5*, 5712. https://doi.org/10.1038/ncomms6712.
62. Marin-Bejar, O., Rogiers, A., Dewaele, M., Femel, J., Karras, P., Pozniak, J., Bervoets, G., Van Raemdonck, N., Pedri, D., Swings, T., et al. (2021). Evolutionary predictability of genetic versus nongenetic resistance to anticancer drugs in melanoma. Cancer Cell *39*, 1135–1149.e8. https://doi.org/10.1016/j.ccell.2021.05.015.
63. Subramanian, A., Narayan, R., Corsello, S.M., Peck, D.D., Natoli, T.E., Lu, X., Gould, J., Davis, J.F., Tubelli, A.A., Asiedu, J.K., et al. (2017). A Next Generation Connectivity Map: L1000 Platform and the First 1,000,000 Profiles. Cell *171*, 1437–1452.e17. https://doi.org/10.1016/j.cell.2017.10.049.
64. Chen, E.Y., Tan, C.M., Kou, Y., Duan, Q., Wang, Z., Meirelles, G.V., Clark, N.R., and Ma'ayan, A. (2013). Enrichr: interactive and collaborative HTML5 gene list enrichment analysis tool. BMC Bioinf. *14*, 128. https://doi.org/10.1186/1471-2105-14-128.
65. Kuleshov, M.V., Jones, M.R., Rouillard, A.D., Fernandez, N.F., Duan, Q., Wang, Z., Koplev, S., Jenkins, S.L., Jagodnik, K.M., Lachmann, A., et al. (2016). Enrichr: a comprehensive gene set enrichment analysis web server 2016 update. Nucleic Acids Res. *44*, W90–W97. https://doi.org/10.1093/nar/gkw377.
66. Xie, Z., Bailey, A., Kuleshov, M.V., Clarke, D.J.B., Evangelista, J.E., Jenkins, S.L., Lachmann, A., Wojciechowicz, M.L., Kropiwnicki, E., Jagodnik, K.M., et al. (2021). Gene Set Knowledge Discovery with Enrichr. Curr. Protoc. *1*, e90. https://doi.org/10.1002/cpz1.90.
67. Verfaillie, A., Imrichova, H., Atak, Z.K., Dewaele, M., Rambow, F., Hulselmans, G., Christiaens, V., Svetlichnyy, D., Luciani, F., Van den Mooter, L., et al. (2015). Decoding the regulatory landscape of melanoma reveals TEADS as regulators of the invasive cell state. Nat. Commun. *6*, 6683. https://doi.org/10.1038/ncomms7683.
68. Robert, C., Grob, J.J., Stroyakovskiy, D., Karaszewska, B., Hauschild, A., Levchenko, E., Chiarion Sileni, V., Schachter, J., Garbe, C., Bondarenko, I., et al. (2019). Five-Year Outcomes with Dabrafenib plus Trametinib in Metastatic Melanoma. N. Engl. J. Med. *381*, 626–636. https://doi.org/10.1056/NEJMoa1904059.
69. Johnson, D.B., Menzies, A.M., Zimmer, L., Eroglu, Z., Ye, F., Zhao, S., Rizos, H., Sucker, A., Scolyer, R.A., Gutzmer, R., et al. (2015). Acquired BRAF inhibitor resistance: A multicenter meta-analysis of the spectrum and frequencies, clinical behaviour, and phenotypic associations of resistance mechanisms. Eur. J. Cancer *51*, 2792–2799. https://doi.org/10.1016/j.ejca.2015.08.022.
70. Kemper, K., Krijgsman, O., Kong, X., Cornelissen-Steijger, P., Shahrabi, A., Weeber, F., van der Velden, D.L., Bleijerveld, O.B., Kuilman, T., Kluin, R.J.C., et al. (2016). BRAF(V600E) Kinase Domain Duplication Identified in Therapy-Refractory Melanoma Patient-Derived Xenografts. Cell Rep. *16*, 263–277. https://doi.org/10.1016/j.celrep.2016.05.064.
71. Song, K., Minami, J.K., Huang, A., Dehkordi, S.R., Lomeli, S.H., Luebeck, J., Goodman, M.H., Moriceau, G., Krijgsman, O., Dharanipragada, P., et al. (2022). Plasticity of Extrachromosomal and Intrachromosomal BRAF Amplifications in Overcoming Targeted Therapy Dosage Challenges. Cancer Discov. *12*, 1046–1069. https://doi.org/10.1158/2159-8290.CD-20-0936.
72. Konieczkowski, D.J., Johannessen, C.M., Abudayyeh, O., Kim, J.W., Cooper, Z.A., Piris, A., Frederick, D.T., Barzily-Rokni, M., Straussman, R., Haq, R., et al. (2014). A melanoma cell state distinction influences sensitivity to MAPK pathway inhibitors. Cancer Discov. *4*, 816–827. https://doi.org/10.1158/2159-8290.CD-13-0424.
73. Anastas, J.N., Kulikauskas, R.M., Tamir, T., Rizos, H., Long, G.V., von Euw, E.M., Yang, P.T., Chen, H.W., Haydu, L., Toroni, R.A., et al. (2014). WNT5A enhances resistance of melanoma cells to targeted BRAF inhibitors. J. Clin. Invest. *124*, 2877–2890. https://doi.org/10.1172/JCI70156.
74. Misek, S.A., Appleton, K.M., Dexheimer, T.S., Lisabeth, E.M., Lo, R.S., Larsen, S.D., Gallo, K.A., and Neubig, R.R. (2020). Rho-mediated signaling promotes BRAF inhibitor resistance in de-differentiated melanoma cells. Oncogene *39*, 1466–1483. https://doi.org/10.1038/s41388-019-1074-1.
75. Richard, G., Dalle, S., Monet, M.A., Ligier, M., Boespflug, A., Pommier, R.M., de la Fouchardière, A., Perier-Muzet, M., Depaepe, L., Barnault, R., et al. (2016). ZEB1-mediated melanoma cell plasticity enhances resistance to MAPK inhibitors. EMBO Mol. Med. *8*, 1143–1161. https://doi.org/10.15252/emmm.201505971.
76. Shaffer, S.M., Dunagin, M.C., Torborg, S.R., Torre, E.A., Emert, B., Krepler, C., Beqiri, M., Sproesser, K., Brafford, P.A., Xiao, M., et al. (2017). Rare cell variability and drug-induced reprogramming as a mode of cancer drug resistance. Nature *546*, 431–435. https://doi.org/10.1038/nature22794.
77. Smith, M.P., Brunton, H., Rowling, E.J., Ferguson, J., Arozarena, I., Miskolczi, Z., Lee, J.L., Girotti, M.R., Marais, R., Levesque, M.P., et al. (2016). Inhibiting Drivers of Non-mutational Drug Tolerance Is a Salvage Strategy for Targeted Melanoma Therapy. Cancer Cell *29*, 270–284. https://doi.org/10.1016/j.ccell.2016.02.003.
78. Lionarons, D.A., Hancock, D.C., Rana, S., East, P., Moore, C., Murillo, M.M., Carvalho, J., Spencer-Dene, B., Herbert, E., Stamp, G., et al. (2019). RAC1(P29S) Induces a Mesenchymal Phenotypic Switch via Serum Response Factor to Promote Melanoma Development and Therapy Resistance. Cancer Cell *36*, 68–83.e9. https://doi.org/10.1016/j.ccell.2019.05.015.
79. Irby, R.B., and Yeatman, T.J. (2000). Role of Src expression and activation in human cancer. Oncogene *19*, 5636–5642. https://doi.org/10.1038/sj.onc.1203912.
80. Westhoff, M.A., Serrels, B., Fincham, V.J., Frame, M.C., and Carragher, N.O. (2004). SRC-mediated phosphorylation of focal adhesion kinase couples actin and adhesion dynamics to survival signaling. Mol. Cell Biol. *24*, 8113–8133. https://doi.org/10.1128/MCB.24.18.8113-8133.2004.
81. Hirata, E., Girotti, M.R., Viros, A., Hooper, S., Spencer-Dene, B., Matsuda, M., Larkin, J., Marais, R., and Sahai, E. (2015). Intravital imaging reveals how BRAF inhibition generates drug-tolerant microenvironments with high integrin beta1/FAK signaling. Cancer Cell *27*, 574–588. https://doi.org/10.1016/j.ccell.2015.03.008.
82. Yen, I., Shanahan, F., Lee, J., Hong, Y.S., Shin, S.J., Moore, A.R., Sudhamsu, J., Chang, M.T., Bae, I., Dela Cruz, D., et al. (2021). ARAF mutations confer resistance to the RAF inhibitor belvarafenib in melanoma. Nature *594*, 418–423. https://doi.org/10.1038/s41586-021-03515-1.
83. Yang, C., Tian, C., Hoffman, T.E., Jacobsen, N.K., and Spencer, S.L. (2021). Melanoma subpopulations that rapidly escape MAPK pathway inhibition incur DNA damage and rely on stress signalling. Nat. Commun. *12*, 1747. https://doi.org/10.1038/s41467-021-21549-x.
84. Yusa, K., Zhou, L., Li, M.A., Bradley, A., and Craig, N.L. (2011). A hyperactive piggyBac transposase for mammalian applications. Proc. Natl. Acad. Sci. USA *108*, 1531–1536. https://doi.org/10.1073/pnas.1008322108.

85. Andrews, S. (2010). FastQC: a quality control tool for high throughput sequence data. http://www.bioinformatics.babraham.ac.uk/projects/fastqc.
86. Bray, N.L., Pimentel, H., Melsted, P., and Pachter, L. (2016). Near-optimal probabilistic RNA-seq quantification. Nat. Biotechnol. *34*, 525–527. https://doi.org/10.1038/nbt.3519.
87. Love, M.I., Huber, W., and Anders, S. (2014). Moderated estimation of fold change and dispersion for RNA-seq data with DESeq2. Genome Biol. *15*, 550. https://doi.org/10.1186/s13059-014-0550-8.
88. Korotkevich, G., Sukhov, V., and Sergushichev, A. (2019). Fast gene set enrichment analysis. Preprint at bioRxiv. https://doi.org/10.1101/060012.
89. Subramanian, A., Tamayo, P., Mootha, V.K., Mukherjee, S., Ebert, B.L., Gillette, M.A., Paulovich, A., Pomeroy, S.L., Golub, T.R., Lander, E.S., and Mesirov, J.P. (2005). Gene set enrichment analysis: a knowledge-based approach for interpreting genome-wide expression profiles. Proc. Natl. Acad. Sci. USA *102*, 15545–15550. https://doi.org/10.1073/pnas.0506580102.
90. Yan, L. (2023). An easy-to-use way to draw pretty venn diagram by 'ggplot2'. https://cran.r-project.org/web/packages/ggvenn/index.html.
91. Yu, G. (2023). enrichplot: Visualization of Functional Enrichment Result. R package version 1.20.1. https://yulab-smu.top/biomedical-knowledge-mining-book/.
92. Yu, G., Wang, L.G., Yan, G.R., and He, Q.Y. (2015). DOSE: an R/Bioconductor package for disease ontology semantic and enrichment analysis. Bioinformatics *31*, 608–609. https://doi.org/10.1093/bioinformatics/btu684.
93. Wilson, M.H., Coates, C.J., and George, A.L., Jr. (2007). PiggyBac transposon-mediated gene transfer in human cells. Mol. Ther. *15*, 139–145. https://doi.org/10.1038/sj.mt.6300028.
94. Colaprico, A., Silva, T.C., Olsen, C., Garofano, L., Cava, C., Garolini, D., Sabedot, T.S., Malta, T.M., Pagnotta, S.M., Castiglioni, I., et al. (2016). TCGAbiolinks: an R/Bioconductor package for integrative analysis of TCGA data. Nucleic Acids Res. *44*, e71. https://doi.org/10.1093/nar/gkv1507.

STAR★METHODS

KEY RESOURCES TABLE

REAGENT or RESOURCE	SOURCE	IDENTIFIER
Antibodies		
α-tubulin	UIOWA hybridoma bank	Catalog #: 12G10
VAV1	Millipore Sigma	Catalog #: AB-174
PDGFRB	CST	Catalog #: 28E1
CSF1R	CST	Catalog #: D3O9X
ERK1/2	CST	Catalog #: 9102
phospho-ERK1/2 (T202/Y204)	CST	Catalog #: 9101
ARAF	CST	Catalog #: 4432
CAV1	CST	Catalog #: 3267S
AXL	CST	Catalog #: C89E7
Chemicals, peptides, and recombinant proteins		
Encorafenib	MedChemExpress	Catalog #: HY-15605
Binimetinib	MedChemExpress	Catalog #: HY-15202
LY3009120	MedChemExpress	Catalog #: HY-12558
Cobimetinib	Selleckchem	Catalog #: S8041
Saracatinib	Selleckchem	Catalog #: S1006
Critical commercial assays		
Viability reagent: Resazurin	Millipore Sigma	Catalog #: R7017
5-alpha Competent *E. coli*	NEB	Catalog #: C2987H
Enzyme: AMV reverse transcriptase	NEB	Catalog #: M0277S
RT-qPCR reagent: EvaGreen	Biotium	Catalog #: 31000
Transfection Reagent: Effectene	Qiagen	Catalog #: 301427
Transfection Reagent: jetOPTIMUS	Polyplus	Reference #: 101000006
RNA extraction kit: Monarch Total RNA Miniprep Kit	NEB	Catalog #: T2010S
Neon Transfection System	Thermofisher	Catalog #: MPK5000S
GenElute Mammalian Genomic DNA Miniprep Kit	Millipore Sigma	Catalog #: G1N350
Minelute 96-well clean-up plate	Qiagen	Catalog #: 28053
Enzyme: Platinum Taq	Thermofisher	Catalog #: 10966018
LMPCR reagent: ATP	Thermofisher	Catalog #: R0441
Enzyme: HpaI	NEB	Catalog #: R0105S
Enzyme: EcoNI	NEB	Catalog #: R0521S
Enzyme: BamH1	NEB	Catalog #: R3136S
Enzyme: dsDNA Fragmentase	NEB	Catalog #: M0348
Enzyme: T4 DNA polymerase	NEB	Catalog #: M0203
Enzyme: T4 DNA ligase	NEB	Catalog #: M0202
Deposited data		
Raw and analyzed RNAseq files	This manuscript	NCBI GEO: GSE226664
Tsoi undifferentiated genes	Tsoi et al.[55]	https://ars.els-cdn.com/content/image/1-s2.0-S1535610818301223-mmc4.xlsx

(*Continued on next page*)

Continued

REAGENT or RESOURCE	SOURCE	IDENTIFIER
Verfaillie TEADs genes	Verfaillie et al.[67]	https://static-content.springer.com/esm/art%3A10.1038%2Fncomms7683/MediaObjects/41467_2015_BFncomms7683_MOESM1479_ESM.xlsx
Experimental models: Cell lines		
Human: A375	American Type Culture Collection (ATCC)	Catalog #: CRL-1619
Human: 451Lu	Rockland Inc.	Catalog #: 451Lu-01-0001
Human: SKMEL28	American Type Culture Collection (ATCC)	Catalog #: HTB-72
Human: UACC257	NCI DCTD Tumor Repository	Catalog #: UACC-257
Human: UACC62	NCI DCTD Tumor Repository	Catalog #: UACC-62
Human: PDX10	University of Iowa MAST	N/A
Oligonucleotides		
Primer: SB100 RT-qPCR F: 5′-AATGGGTCTTCCAACACGAC-3′	Feddersen et al.[11]	N/A
Primer: SB100 RT-qPCR R: 5′-GTGATGGCCACTCCAATACC-3′	Feddersen et al.[11]	N/A
Primer: TBP RT-qPCR F: 5′-TTCGGAGAGTTCTGGGATTG-3′	Feddersen et al.[11]	N/A
Primer: TBP RT-qPCR R: 5′-CTCATGATTACCGCAGCAAA-3′	Feddersen et al.[11]	N/A
Linker+: 2021: 5′- GTACCCATACGA CGTCCCAGACTCCGCTTAAGGGAC-3′	This paper	N/A
Linker-: 2021: 5′-Phos-GTCCCTTAAG CGGAG-C3spacer-3′	This paper	N/A
Primer: Primary PCR IRR: 2021: 5′-GGATTAAATGTCAGGAATTGTGAAAA- 3′	This paper	N/A
Primer: Primary PCR IRL: 2021: 5′-GGATTAAATGTCAGGAATTGTGAAAA- 3′	This paper	N/A
Primer: Primary PCR linker: 2021: 5′-TACCCATACGACGTCCCAGA-3′	This paper	N/A
Linker+: 2019: 5′-GTAATACGACTCACTA TAGGGCTCCGCTTAAGGGAC-3′	Feddersen et al.[11]	N/A
Linker-: 2019: 5′-Phos-GTCCCTTAAG CGGAG-C3spacer-3′	Feddersen et al.[11]	N/A
Primer: Primary PCR linker 2019: 5′-GTAATACGACTCACTATAGGGC-3′	Feddersen et al.[11]	N/A
Primer: Primary PCR IRL V1.1: 5′-TCGTCGGCAGCGTCAGATGT GTATAAGAGACAGHAAATTTGT GGAGTAGTTGAAAAACGA-3′	Feddersen et al.[11]	N/A
Primer: Primary PCR IRL V1.2: 5′- TCGTCGGCAGCGTCAGATG TGTATAAGAGACAGNCAAATTT GTGGAGTAGTTGAAAAACGA-3′	Feddersen et al.[11]	N/A
Primer: Primary PCR IRL V1.3: 5′-TCGTCGGCAGCGTCAGATGT GTATAAGAGACAGNNYAAATTT GTGGAGTAGTTGAAAAACGA-3′	Feddersen et al.[11]	N/A

(*Continued on next page*)

Continued

REAGENT or RESOURCE	SOURCE	IDENTIFIER
Primer: Primary PCR IRL V1.4: 5′- TCGTCGGCAGCGTCAGATG TGTATAAGAGACAGNNYCAAA TTTGTGGAGTAGTTGAAAAACGA-3′	Feddersen et al.[11]	N/A
Primer: Primary PCR IRL V1.5: 5′- TCGTCGGCAGCGTCAGATGT GTATAAGAGACAGNNNBCCAAA TTTGTGGAGTAGTTGAAAAACGA-3′	Feddersen et al.[11]	N/A
Primer: Primary PCR IRR V1.1: 5′- TCGTCGGCAGCGTCAGATGTG TATAAGAGACAGHGGATTAAATG TCAGGAATTGTGAAAA-3′	Feddersen et al.[11]	N/A
Primer: Primary PCR IRR V1.2: 5′- TCGTCGGCAGCGTCAGATGTG TATAAGAGACAGNNGGATTAAAT GTCAGGAATTGTGAAAA-3′	Feddersen et al.[11]	N/A
Primer: Primary PCR IRR V1.3: 5′- TCGTCGGCAGCGTCAGATGTG TATAAGAGACAGNNYGGATTAAA TGTCAGGAATTGTGAAAA-3′	Feddersen et al.[11]	N/A
Primer: Primary PCR IRR V1.4: 5′- TCGTCGGCAGCGTCAGATGT GTATAAGAGACAGNNNYGGATT AAATGTCAGGAATTGTGAAAA-3′	Feddersen et al.[11]	N/A
Primer: Primary PCR IRR V1.5: 5′- TCGTCGGCAGCGTCAGATGT GTATAAGAGACAGNNNYCGGAT TAAATGTCAGGAATTGTGAAAA-3′	Feddersen et al.[11]	N/A
Primer: Primary PCR LINK V1.1 2019: 5′- TCGTCGGCAGCGTCAGATGTG TATAAGAGACAGGTAATACGACT CACTATAGGGC-3′	Feddersen et al.[11]	N/A
Primer: Primary PCR LINK V1.2 2019: 5′- TCGTCGGCAGCGTCAGATGTGT ATAAGAGACAGHNGTAATACGACT CACTATAGGGC-3′	Feddersen et al.[11]	N/A
Primer: Primary PCR LINK V1.3 2019: 5′- TCGTCGGCAGCGTCAGATGTGT ATAAGAGACAGNNYBGTAATACGA CTCACTATAGGGC-3′	Feddersen et al.[11]	N/A
Primer: Primary PCR LINK V1.4 2019: 5′- TCGTCGGCAGCGTCAGATGTGT ATAAGAGACAGNNYBCNGTAATAC GACTCACTATAGGGC-3′	Feddersen et al.[11]	N/A
Primer: Primary PCR LINK V1.5 2019: 5′- TCGTCGGCAGCGTCAGATGTGT ATAAGAGACAGNNYBCNCCCGTAA TACGACTCACTATAGGGC-3′	Feddersen et al.[11]	N/A

(*Continued on next page*)

Continued

REAGENT or RESOURCE	SOURCE	IDENTIFIER
Primer: Primary PCR LINK V1.1 2021: 5′- TCGTCGGCAGCGTCAGATGTGTA TAAGAGACAGTACCCATACGACGT CCCAGA-3′	This paper	N/A
Primer: Primary PCR LINK V1.2 2021: 5′- TCGTCGGCAGCGTCAGATGTGTA TAAGAGACAGHNTACCCATACGAC GTCCCAGA-3′	This paper	N/A
Primer: Primary PCR LINK V1.3 2021: 5′- TCGTCGGCAGCGTCAGATGTGT ATAAGAGACAGNNYBTACCCATAC GACGTCCCAGA-3′	This paper	N/A
Primer: Primary PCR LINK V1.4 2021: 5′- TCGTCGGCAGCGTCAGATGTG TATAAGAGACAGNNYBCNTACCC ATACGACGTCCCAGA-3′	This paper	N/A
Primer: Primary PCR LINK V1.5 2021: 5′- TCGTCGGCAGCGTCAGATGTGT ATAAGAGACAGNNYBCNCCCTAC CCATACGACGTCCCAGA-3′	This paper	N/A
Primer: Secondary PCR Nextera XT index	Illumina	Catalog #: FC-131-2001, FC-131-2002, FC-131-2003, FC-131-2004
Recombinant DNA		
Plasmid: pT2-Onc3	Feddersen et al.[11]	N/A
Plasmid: PB-EF1α-SB100	Feddersen et al.[11]	N/A
Plasmid: hyPBase	Yusa et al.[84]	N/A
Plasmid: PB-EF1α-VAV1	This paper	N/A
Plasmid: PB-EF1α-PDGFRB	This paper	N/A
Plasmid: PB-EF1α-CSF1R	This paper	N/A
Plasmid: PB-EF1α-PDGFRB^{N666K}	This paper	N/A
Plasmid: PB-EF1α-CSF1R $^{L301S,\ Y969}$	This paper	N/A
Software and algorithms		
FastQC	S. A. and Bittencourt A[85]	https://www.bioinformatics.babraham.ac.uk/projects/fastqc/
Kallisto	Bray et al.[86]	https://pachterlab.github.io/kallisto/download
Deseq2	Love et al.[87]	https://bioconductor.org/packages/release/bioc/html/DESeq2.html
fgsea	Korotkevich et al.[88]	https://github.com/ctlab/fgsea
GSEA	Subramanian et al.[89]	https://www.gsea-msigdb.org/gsea/index.jsp
ggvenn	Yan L.[90]	https://cran.r-project.org/web/packages/ggvenn/index.html.
Enrichr	Chen et al.,[64]; Kuleshov et al.,[65] and Xie et al.[66]	https://maayanlab.cloud/Enrichr/
enrichplot	Yu[91]	https://bioconductor.org/packages/release/bioc/html/enrichplot.html
DOSE	Yu et al.[92]	https://bioconductor.org/packages/release/bioc/html/DOSE.html
Analysis scripts	This manuscript	https://github.com/eyzhu/SB_Melanoma_BRAFi

RESOURCE AVAILABILITY

Lead contact

Further information and requests for resources and reagents should be directed to and will be fulfilled by the lead contact, Adam J. Dupuy (adam-dupuy@uiowa.edu).

Materials availability

This study did not generate new unique reagents.

Data and code availability

- RNAseq data generated from this study can be obtained from GEO (accession no. GSE226664) and are publicly available.
- Custom code used to analyze the RNAseq data can be obtained from GitHub (https://github.com/eyzhu/SB_Melanoma_BRAFi) and are publicly available.
- Any additional information required to reanalyze the data reported in this paper is available from the lead contact upon request.

EXPERIMENTAL MODEL AND STUDY PARTICIPANT DETAILS

Cell lines

A375, 451Lu, COLO858, and SKMEL28 were obtained from ATCC. UACC257 was obtained from NCI cell line repository. PDX10 was obtained from a patient-derived xenograft model of cutaneous melanoma. PDX10 habors *BRAF*^{V600E} and has wild-type *NRAS*. Informed consent was obtained from patient to create PDX10 for research use. PDX10 was confirmed to be a human cell line via STR analysis. A375 and 451Lu were cultured in Gibco DMEM, supplemented with penicillin/streptomycin, and 10% FBS. SKMEL28 was cultured in Gibco DMEM, supplemented with penicillin/streptomycin, 10% FBS, Sodium pyruvate, and non-essential amino acids. COLO858, PDX10, and UACC257 were cultured in Gibco RPMI, supplemented with penicillin/streptomycin, and 10% FBS.

METHOD DETAILS

Sleeping beauty genetic screens

Cells were first stably transfected with *SB100* using the *piggyBac* transposon/transposase system.[84,93] Following, cells were transfected with the pT2-On3 transposon either with Qiagen Effectene (4ug DNA for 10 cm dish, 1:8 enhancer and 1:10 effectene ratios) for A375 and COLO858, Jet OPTIMUS (10ug DNA for 10 cm dish, 10 uL reagent) for PDX10, or the Neon electroporation system (100 uL tip, 10 ug DNA, 1200 V, 20 ms, 2 pulses) for UACC62 and UACC257. Two days following transfection, one million cells for A375, COLO858, and PDX10 or two million cells for UACC62 and UACC257 were seeded in a 10CM dish. One day after seeding, cells were either treated with DMSO for 3-5 days or with ENCOR and COBI for 3-5 weeks until colonies formed. For each cell line, a screen consisted of 13-28 BRAF/MEK inhibitor treated plates and 9-10 DMSO treated plates. The concentration of ENCOR/BINI used were 500/50 nM for A375, 10/2 nM for COLO858, 8/2 nM for UACC62, 60/6 nM for PDX10, and 18/2 nM for UACC257. The concentration of LY3009120 used were 130 nM for A375 and 38 nM for COLO858.

Library preparation and sequencing

Genomic DNA was extracted using the sigma GenElute Mammalian Genomic DNA Miniprep Kit (G1N350). Instructions to perform transposon targeted sequencing can be obtained from Github. A375 and COLO858 samples were prepared using the 2021 protocol while UACC257, UACC62, and PDX10 samples were prepared using the 2022 protocol.

Cell staining

10 cm plates were first rinsed with PBS. Following, cells were fixed with ice cold 70% ethanol. Plates were then coated with Coomassie blue stain and allowed to rest for 5 minutes. Finally, plates were rinsed with tap water.

RT-qPCR

The following primers were used to perform RT-qPCR on the indicated targets: SB100X (5′-AATGGGTCTTCCAACACGAC-3′, 5′-GTGATGGCCACTCCAATACC-3′) and TBP (5′-TTCGGAGAGTTC TGGGATTG-3′, 5′-CTCATGATTACCGCAGCAAA-3′). cDNA was synthesized using NEB AMV reverse transcriptase (M0277S). RT-qPCR was performed using Taq polymerase with EvaGreen dye with total reaction volume of 12 uL. Three technical replicates were obtained for each sample. Samples were run on the BioRad CFX Real-Time PCR Detection System.

Enforced expression of candidates

Cloned cDNAs of candidate genes were inserted into a *piggyBac* transposon expression vector and co-transfected with the *piggyBac* transposase at a 5:1 ratio (transposon-to-transposase). Transfections were performed in a six-well format. Qiagen Effectene (0.8ug DNA, 1:8

enhancer and 1:10 effectene ratios) for A375 and 451Lu, Jet OPTIMUS (2ug DNA and 2 uL reagent) for PDX10, or the Neon electroporation system (100 uL tip, 10 ug DNA, 1200 V, 20 ms, 2 pulses) for SKMEL28. Media was changed 24 hours after transfection. Cells were split into 10 cm cell culture dishes 48 hours post-transfection. 72 hours post-transfection, cells were selected with puromycin for six days with antibiotic changes every 48 hours. The concentration of puromycin used was 0.8 ug/mL for A375 and 451Lu, 1 ug/mL for PDX10, and 0.6 ug/mL for SKMEL28. The cell lines we used for validation were chosen because we had previously characterized their differentiation status.[46]

Viability assays

Drug dose response curves were generated using the resazurin assay. Viability at each dose was measured in triplicate. Cells were seeded in a 96-well plate. Cells were treated with drug 24 hours later. Data shown represents fluorescent signal detected at day 3 or 4 either normalized to the vehicle treated wells at the endpoint or at day 0. The assay was performed by putting 100 uL of cell culture media and 20 uL of 6x stock (0.15mg/ml) of resazurin onto cells, followed by a 2 hour incubation at 37-degrees in a tissue culture incubator. Plates were acquired using the Biotek Synergy HT microplate reader and Gen5 software.

Inhibitors

Encorafenib (LGX818), Binimetinib (ARRY-162), and LY3009120 were obtained from MedChemExpress, Cobimetinib (GDC-0973) and Saracatinib (AZD0530) was obtained from Selleckchem.

Immunoblotting

Whole-cell lysates were separated on Tris-Glycine 4-20% gradient gels (Thermofisher) or hand-cast SDS-PAGE gels and transferred to nitrocellulose or PVDF membranes overnight. The blots were blocked in Odyssey Blocking Buffer PBS (Licor) for 1 hour and incubated with primary antibodies overnight at 4 degrees followed by 1h incubation at room temperature with secondary antibodies. Blots were imaged using the Odyssey 9210 (Licor). The antibodies we used were alpha-tubulin (12G10 UIOWA hybridoma bank), ARAF (CST 4432), VAV1 (Sigma AB-174), PDGFRB (CST 28E1), CSF1R (CST D3O9X), ERK1/2 (CST 9102), p-ERK1/2 (CST 9101), CAV1 (CST 3267S), and AXL (CST C89E7). Blots to confirm overexpression were performed with technical duplicates. Blots to determine p-ERK levels were performed with technical triplicates.

QUANTIFICATION AND STATISTICAL ANALYSIS

RNAseq analysis

FastQC was used to determine the quality of the fastq files.[85] Transcript alignment/quantification was performed with Kallisto using default settings.[86] Ensembl annotation v86 was used as the reference transcriptome. Differential expression analysis was performed using Deseq2 with default settings.[87] Enrichment analysis was performed using the fgsea, enrichplot, DOSE, and GSEA R packages.[88,89,91,92] Genes were ranked using the log2 fold change (log_2FC). Benjamini-Hochberg was used to compute the adjusted p values. The Venn diagram in Figure 4C was made using the ggvenn R package.[90]

The Tsoi 2018 Undifferentiated gene set included 224 genes belonging to "undifferentiated" and "undifferentiated-neural crest like" listed in Table S3 of Tsoi et al.[55] The Verfaillie-TEADs gene set was obtained from Supplementary Data 3 from Verfaillie et al.[67] Enrichr was used to generate the LINCs L1000 chemical perturbation consensus signatures for the indicated gene sets.[64–66]

Transposon insertion site analysis

We used our gene-centric common insertion site analysis to determine the statistical significance of insertions.[12,18] This method relies on a chi-squared test based on the observed and expected number of insertions in a gene. The expected number of insertions in a gene is derived from the number of TA sites in a gene and the total number of insertions in the dataset.

TCGA analysis

TCGA patient data was extracted from the TCGA SKCM dataset using the GDCquery function in the TCGAbiolinks R package.[94] The settings for GDCquery were project = "TCGA-SKCM", data.category = "Transcriptome Profiling", data.type = "Gene Expression Quantification", and workflow.type = "HTSeq - Counts". These counts were normalized using the DESeqDataSetFromMatrix function with default settings. Patients were assigned to either the differentiated or de-differentiated class based on k-means clustering k=2 of ~400 genes that define the de-differentiated cutaneous melanoma subtype described in our previous paper.[67]

Statistical analysis

Specific details on the statistical tests performed are provided in figure captions.